



Cooperative situational awareness of multi-UAV system based on improved D-S evidence theory



Zirui Liao ^{a,b,d,e}, Shaoping Wang ^{a,b,c}, Jian Shi ^{a,b,*}, Zhiyong Sun ^d, Yuwei Zhang ^{a,b}, Muhammad Baber Sial ^{a,b}

^a School of Automation Science and Electrical Engineering, Beihang University, Beijing, 100191, China

^b Beijing Advanced Innovation Center for Big-Data Based Precision Medicine, Beihang University, Beijing, 100191, China

^c Tianmushan Laboratory, Hangzhou, 310023, China

^d Department of Electrical Engineering, Eindhoven University of Technology, Eindhoven, 5600 MB, Netherlands

^e Shenyuan Honors College, Beihang University, Beijing, 100191, China

ARTICLE INFO

Article history:

Received 2 December 2022

Received in revised form 29 June 2023

Accepted 30 August 2023

Available online 6 September 2023

Communicated by Qinglei Hu

Keywords:

Multi-UAV system

Situational awareness

Information fusion

Modified D-S evidence theory

ABSTRACT

Situational awareness (SA) of unmanned aerial vehicles (UAVs) has been a research hotspot over the decades. Existing research mainly focuses on the SA of a single UAV in two-dimensional planes, whereas obstacles are assumed *a priori*. To eliminate these constraints, this study considers the cooperative situational awareness (CSA) problem of multi-UAV systems in the scenario of crossing a three-dimensional (3D) obstacle belt while no prior information of obstacles is required. First, the distribution models of the multi-UAV system and the obstacles are built based on two reference frames. Second, various types of uncertainties are characterized, which reflect an urgent need for CSA. Thus, a centralized CSA scheme is proposed and conducted on multiple UAVs and at different times, and the Dempster-Shafer (D-S) evidence theory is introduced to address information uncertainties and achieve high-accuracy information fusion. Next, to deal with the high-conflict evidence situations that are common in practice, a modified D-S fusion method is further developed. A modified Pearson coefficient is utilized to measure the correlation between different pieces of evidence. Both information credibility and uncertainty are taken into account to evaluate the evidence from different perspectives, and a novel evidence weight assignment method is presented to treat high-conflict situations. Numerical simulations validate the effectiveness of the proposed CSA method. Compared to existing studies, the proposed method is applicable to different trust paradoxes and achieves the best performance among various fusion methods.

© 2023 Elsevier Masson SAS. All rights reserved.

1. Introduction

Situational awareness (SA) is the perception of the elements in the environment within a volume of time and space [1], which lays a solid basis for UAV networks to implement a wide variety of missions. Accurate SA is an essential challenge to unleash UAV's potential for practical applications [2]. Moreover, SA is critical for the reliable operation of almost all systems and domains [3–5]. In the aviation industry, SA is one of the vital elements in pilot training for flying, controlling, and maintaining [6]. The requirements for reliable UAV control and SA are explained in [7], which states

that all nodes should periodically broadcast a precise participant location and identification message (e.g., position and state).

Although numerous studies have applied UAVs for SA, the strong uncertainty in the environment can easily lead to inaccurate SA results [8]. Moreover, in the perception system of UAV, the quantity and quality of detection data directly affect the effectiveness of SA, thus suggesting the significance of information acquisition and processing [9,10]. In [11], a UAV-based situational awareness system using deep learning was built to detect and locate people and recognize their actions in near real-time. However, the accuracy of action recognition was affected by the accuracy of the person detection, resulting in a low mean Average Precision (mAP). Furthermore, single visual camera, which is commonly used as a device for situational awareness, has limited ability to obtain complete information of objects [11]. Accordingly, a multi-UAV system with multiple visual cameras is expected to improve the quantity and quality of information acquisition, obtain accurate environmental information, and achieve precise cooperative situa-

* Corresponding author at: School of Automation Science and Electrical Engineering, Beihang University, Beijing, 100191, China.

E-mail addresses: by2003110@buaa.edu.cn (Z. Liao), shaopingwang@buaa.edu.cn (S. Wang), shijian@buaa.edu.cn (J. Shi), z.sun@tue.nl (Z. Sun), zhangyuwei@buaa.edu.cn (Y. Zhang), babersial@buaa.edu.cn (M.B. Sial).

Nomenclature

\mathbf{p}_i	Position of UAV i in earth-fixed coordinate frame	$P(\alpha)$	Correlation between detection accuracy and visual angle
Φ_j	Obstacle j	$P_A(L, \alpha)$	Overall detection accuracy
$\mathbf{p}_b(\Phi_j)$ and $\mathbf{p}_e(\Phi_j)$	Position of obstacle j in body-fixed and earth-fixed coordinate frame	$m(L_t, \alpha_t)$	Basic probability assignment function of information fusion
$\delta_i = [\theta_i, \varphi_i, \psi_i]^T$	Attitude angle set of UAV i	$\mathbf{p}_1(\Phi_1)$	Position of detected by UAV I
\mathbf{T}_{be}	Translation vector	$m_1(\Phi_1)$	Detection accuracy of detected by UAV I
\mathbf{R}_{be}	Rotation matrix	$\mathbf{P}_{123}(\Phi_1)$	Fused position of Φ_1 among UAV I, II and III
\mathbf{v}_i	Velocity vector of UAV i	$\mathbf{p}^{t_1}(\Phi_1)$	Position of detected at time t_1
L_s	Superior limit of visual distance L	$m^{t_1}(\Phi_1)$	Detection accuracy of Φ_1 detected at time t_1
α_s	Superior limit of visual angle α	$\mathbf{P}^{t_1 t_2 t_3}(\Phi_1)$	Fused position of Φ_1 among time t_1, t_2 and t_3
Θ	Discernment frame	$\rho_M(m_i, m_j)$	The modified Pearson coefficient between evidence m_i and m_j
$m(\Phi)$	Basic probability assignment function	$\text{Sup}(m_i)$	Support degree of evidence m_i
k	Conflict coefficient	$\text{Crd}(m_i)$	Credibility of evidence m_i
$P(L)$	Correlation between detection accuracy and visual distance	$\text{Un}(m_i)$	Uncertainty degree of evidence m_i

tional awareness (CSA). As a key factor in multi-UAV cooperative operation, the CSA of multi-UAV systems has also attracted extensive attention in relevant fields [12–14], which requires that the information obtained by all UAVs achieve a consensus with true environmental information [15].

The CSA is capable of reducing or eliminating the effect of uncertainty through the interaction of information, i.e., the multi-sensor information fusion. Multi-sensor information fusion technology refers to processing the data transmitted from different information sources, combining the above data according to certain rules, and then making efficient and accurate decisions [16]. It is a rapidly developing discipline and has been applied to a wide variety of scenarios including the SA [17–19]. Theoretical multi-sensor information fusion methods include the weighted average method [20], Kalman filter method [21], Bayesian estimation method [22,23], D-S evidence theory [24–26], etc. Nevertheless, a common feature of the most existing work on CSA is to assume the environment information to be *a priori* and ideal airborne sensors, while the uncertainty caused by unknown obstacles, sensor aging, and interference from other factors in CSA often leads to abnormal information and inaccurate CSA results. Ref. [27] presented a multi-UAV cooperation method via workflow, in which the authors clarified that the situational synchronization of detected targets among UAVs could be achieved through limited information interactions, but the information uncertainty was not thoroughly considered. In [15], a multi-UAV CSA consensus three-level model was built considering the information uncertainty; however, this kind of uncertainty was only reflected in the reference matrices without specific modeling and characterization. It is noteworthy that though Bayesian estimation method is also capable of solving information uncertainty, it requires previous data as *a priori* probability to obtain a novel probability, which is not applicable in numerous cases [28]. In contrast, D-S evidence theory is capable of fusing uncertain information when the prior probability is unknown and representing the probability of uncertain problems using the basic probability assignment, thus indicating the superior fusion performance of the theory. Due to its advantages, D-S evidence theory has been employed in a wide variety of areas to solve related problems, especially in the CSA field. In [29], a situational assessment mathematical model based on the D-S evidence theory has been studied. Moreover, D-S evidence theory is combined in [30] to improve the accuracy of ship target type recognition, which is greatly associated with battlefield SA. Considering its excellent performance in dealing with sensor uncertainty, the D-S

evidence theory is adopted as the multi-sensor information fusion method in this study to achieve CSA of multi-UAV systems.

In addition, though the conventional D-S evidence theory is capable of dealing with the uncertainty in CSA, it still has limitations in trust paradox, one-vote rejection, etc. The trust paradox reveals that contrary results may be obtained in the presence of high-conflict evidence. To address the above problems, scholars have improved the conventional D-S evidence theory from different perspectives [31], which are mainly divided into two categories: the improved D-S combination rules and the modified conflict evidence methods. Some researchers think that unreasonable results are mainly caused by the normalization step of D-S combination rule. Thus, they optimize the D-S combination rule by giving evidence conflicts to a certain subset with a specific proportion, which is called the improved D-S combination rule. In [32], the uncertain domain is considered an incomplete set and conflicts are given to an unknown proposition. This method solves paradoxes theoretically, whereas it increases the uncertainty of synthesis results by introducing an unknown proposition. Yager in [33] allotted conflicts directly to the uncertain domain. However, it can only settle paradoxes efficiently with two evidence sources, and it is too conservative to admit the useful information that exists in conflict evidence. On this basis, an improved method is developed by dividing evidence into support evidence and conflicting evidence, which solves the problem of unequal information quantity in evidence [34]. Other scholars consider that paradoxes are mainly caused by unreliable evidence. Thus, instead of changing the D-S combination rule, this type of method modifies evidence before combining evidences, which is called the modified conflict evidence method. To be specific, an improved method is put forward by considering the average mean of evidence as a novel evidence before evidence combination [35]. Note that the idea only averages the evidence without considering their differences. Thus, the paper [36] proposed a fusion method through calculating novel evidence by the weighted sum of evidence. To combine high-conflict evidence efficiently, a novel method is developed in [37] through the introduction of sensor priority and evidence credibility, thus enhancing the reliability of the system.

Motivated by the above observations, this study aims to present a CSA approach based on multi-sensor information fusion. The distribution models of the multi-UAV system and obstacles are established considering multiple uncertainties based on the background of the multi-UAV system detecting an obstacle belt. Subsequently, the D-S evidence theory is applied and modified into the information fusion process to deal with the uncertainties and fuse the

information from the multi-UAV system, such that a more accurate CSA is achieved. The main contributions of this study are presented as follows:

1. A novel centralized CSA scheme based on the idea of information interaction and fusion is proposed and applied to cooperative detection scenarios. No prior information for obstacles is required, i.e., the obstacles can be randomly distributed in a given 3D space. Compared to SA by a single UAV, the proposed CSA scheme enables the multi-UAV system to detect more obstacles, while greatly improving the overall detection accuracy.
2. Unlike previous works [15,27] that ignored the uncertainties thoroughly during the detection process, the proposed CSA scheme integrates various typical uncertainties including the environmental uncertainty, detection uncertainty, and information uncertainty. The D-S evidence theory is introduced and conducted on multiple UAVs and different times to fuse the uncertain information and obtain the detection results with high accuracy.
3. To deal with the aforementioned uncertainties, a modified CSA scheme based on the modified Pearson correlation coefficient is further presented. Thanks to the comprehensive consideration of evidence credibility and uncertainty, the proposed modified CSA scheme is applicable to treat high-conflict situations and outperforms existing research methods [33–35,37] in solving various trust paradoxes.

The remaining sections of the paper are arranged as follows. The coordinate frames and their transformation are defined in Section 2, while the mathematical models of UAV and obstacles are built considering the detection uncertainty and the framework of the D-S evidence theory is established. Section 3 describes the overall process of multi-UAV system CSA among multiple UAVs and different times, while the defects and modifications of the conventional D-S evidence theory are elaborated. Three simulation cases are conducted, and numerical results are displayed in Section 4. Lastly, conclusions and future work are presented in Section 5.

2. Preliminaries

2.1. Coordinate definition and transformation

Definition 1 (*Body and earth-fixed coordinate frames*). To start with, two reference frames are defined, i.e., the body-fixed coordinate frame and the earth-fixed coordinate frame [38]. As depicted in Fig. 1, the body-fixed coordinate frame is a moving coordinate frame which is fixed to the UAV. The origin \mathbf{O}_b is chosen to coincide with the center of gravity, and \mathbf{X}_b , \mathbf{Y}_b , \mathbf{Z}_b represent the \mathbf{X} , \mathbf{Y} , \mathbf{Z} axis of the frame, respectively. Note that the positive direction of \mathbf{X}_b is the head of UAV, the \mathbf{Y}_b axis is perpendicular to the horizontal plane, and the \mathbf{Z}_b axis is perpendicular to the $\mathbf{X}_b\mathbf{O}_b\mathbf{Y}_b$ plane. The earth-fixed coordinate frame, on the other hand, has its origin \mathbf{O}_e fixed to a specific point in space, while \mathbf{X}_e , \mathbf{Y}_e , \mathbf{Z}_e represent its three axes. The motion of UAVs and the location of obstacles are described in this earth-fixed coordinate. For convenience, we abbreviate the obstacle as OBS.

Let $\mathbf{p}_i = [p_i^x, p_i^y, p_i^z]^T \in \mathbb{R}^3$ be the position of UAV i in earth-fixed coordinate frame, while the position of obstacle Φ_j in body and earth-fixed coordinate frames are defined as $\mathbf{p}_b(\Phi_j) = [p_b^x(\Phi_j), p_b^y(\Phi_j), p_b^z(\Phi_j)]^T \in \mathbb{R}^3$ and $\mathbf{p}_e(\Phi_j) = [p_e^x(\Phi_j), p_e^y(\Phi_j), p_e^z(\Phi_j)]^T \in \mathbb{R}^3$, respectively. In addition, $\delta_i = [\phi_i, \theta_i, \psi_i]^T \in \mathbb{R}^3$ denotes the attitude angles set of UAV i , where ϕ_i , θ_i and ψ_i are roll, pitch and yaw angles of UAV i , respectively. The solid blue

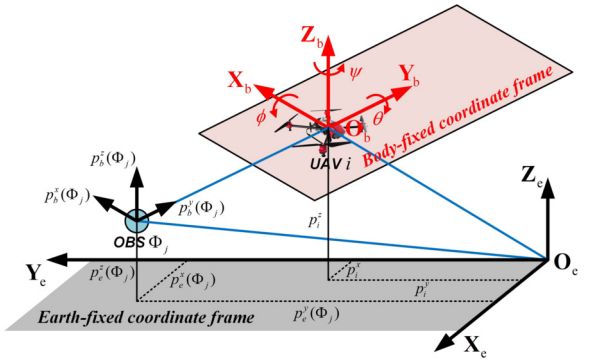


Fig. 1. Body and earth-fixed coordinate frame. (For interpretation of the colors in the figure(s), the reader is referred to the web version of this article.)

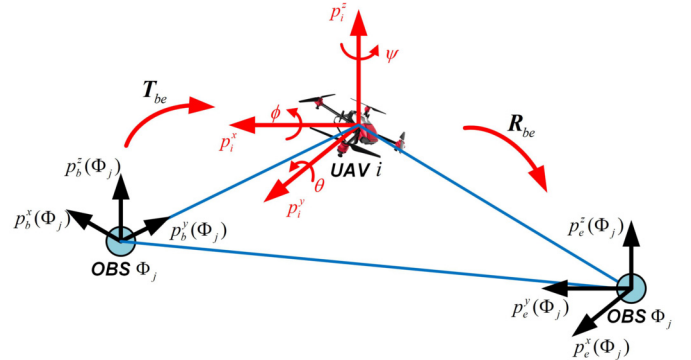


Fig. 2. Transformation from body-fixed coordinate to earth-fixed coordinate.

line represents the transformation between the body-fixed coordinate frame and the earth-fixed coordinate frame, which will be precisely described in Fig. 2.

Remark 1. The initial information available for ground base station includes the position of UAV in earth-fixed coordinate frame \mathbf{p}_i , the attitude angle set δ_i and the position of obstacle in body-fixed coordinate frame $\mathbf{p}_b(\Phi_j)$, while the obstacle position in earth-fixed coordinate frame $\mathbf{p}_e(\Phi_j)$ requires the coordinate transformation.

To describe the obstacles in a unified coordinate frame, the obstacle position should be converted from body-fixed coordinate frame to earth-fixed coordinate frame, which is shown in Fig. 2 (the meanings of the symbols in Fig. 2 are the same as those in Fig. 1). As depicted in Fig. 2, the coordinate transformation is achieved through a translation and rotation, which is written as follows:

$$\mathbf{p}_e(\Phi_j) = \mathbf{T}_{be} \cdot \mathbf{R}_{be} \quad (1)$$

where the translation vector $\mathbf{T}_{be} = \mathbf{p}_b(\Phi_j) + \mathbf{p}_i$, and the rotation matrix \mathbf{R}_{be} can be calculated by attitude angles.

2.2. Multi-UAV system and obstacle model

Consider n ($n \geq 2$) UAVs conducting a detection task in \mathbb{R}^3 . The configuration of the multi-UAV system is denoted by $\mathbf{p} = [\mathbf{p}_1^T, \mathbf{p}_2^T, \dots, \mathbf{p}_n^T]^T \in \mathbb{R}^{3n}$, and the kinematics of the UAV can be expressed as $\mathbf{v}_i = \dot{\mathbf{p}}_i$, where $\mathbf{v}_i = [v_i^x, v_i^y, v_i^z]^T \in \mathbb{R}^3$ is the velocity vector of UAV i . The m ($m \geq 2$) obstacles $\Phi = \{\Phi_1, \Phi_2, \dots, \Phi_m\}$ are spatially distributed with $p(\Phi) = [\mathbf{p}^T(\Phi_1), \mathbf{p}^T(\Phi_2), \dots, \mathbf{p}^T(\Phi_m)]^T \in \mathbb{R}^{3m}$ in a given 3D space. Note that the formation of

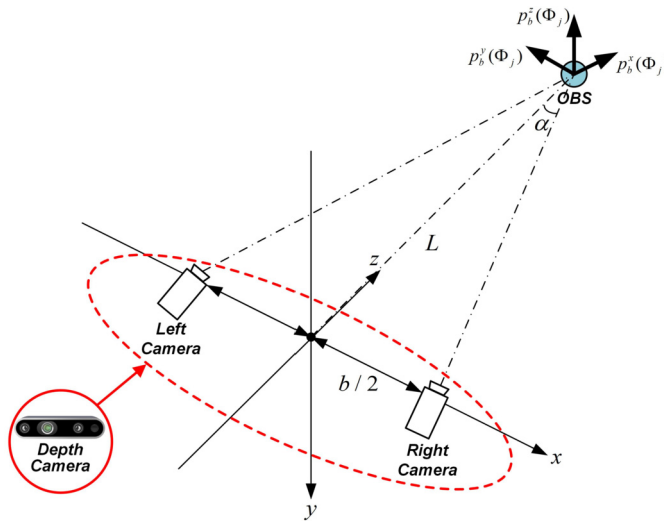


Fig. 3. Obstacle detection by depth camera.

the multi-UAV system is fixed, while the obstacles are randomly distributed in a given 3-D space. In addition, the following assumptions are made.

Assumption 1. The respective UAV carries a limited-capability depth camera which can detect the 3D coordinate of the obstacle within a perception range, as shown in Fig. 3. The detected information includes $\mathbf{p}_b(\Phi_j)$, relative distance L and visual angle α , with $b/2$ representing the focal length of the camera.

Assumption 2. Detection uncertainty occurs during the process of perception, especially when an obstacle deviates from the center of sight and is far away from the UAV's depth camera.

Assumption 3 (Scenario assumption). We consider several UAVs flying forward at speed v_i and perceiving an obstacle belt consisting of multiple obstacles, whereas all UAVs are distributed in the same plane. In accordance with Assumptions 1 and 2, the respective UAV can obtain local and inaccurate information about the obstacle belt merely due to limited detection capability and detection uncertainty. Thus, it is necessary and essential to incorporate the whole information through information fusion to achieve CSA. Fig. 4 presents the diagram.

Definition 2 (Detection capability). The airborne sensor has a certain detection range in practice. As depicted in Fig. 4, for depth camera, its detection range is determined by the superior limit of visual

distance L_s and visual angle α_s , while the relative distance L and visual angle α between UAV and obstacle can be calculated by

$$L = \sqrt{(p_e^x(\Phi_j) - p_i^x)^2 + (p_e^y(\Phi_j) - p_i^y)^2 + (p_e^z(\Phi_j) - p_i^z)^2}, \\ \alpha = \arctan[(p_e^y(\Phi_j) - p_i^y) / (p_e^x(\Phi_j) - p_i^x)], \quad (2)$$

where $p_e^x(\Phi_j), p_e^y(\Phi_j), p_e^z(\Phi_j)$ are the position components of the obstacle Φ_j in the earth-fixed coordinate frame, and p_i^x, p_i^y, p_i^z are the position components of the UAV i in the earth-fixed coordinate frame.

In accordance with Assumption 1, the obstacles can be detected only when they are within the detection range of sensors. In this study, the step function $\delta(L, \alpha)$ is introduced to express the process as follows:

$$\delta(L, \alpha) = \begin{cases} 1, & \text{if } 0 \leq L \leq L_s \text{ and } -\alpha_s \leq \alpha \leq \alpha_s, \\ 0, & \text{otherwise.} \end{cases} \quad (3)$$

2.3. Framework of the D-S evidence theory

The obstacle position and detection accuracy obtained by different UAVs may have conflicts, especially when UAV is at a certain distance from the obstacle. The framework of D-S evidence theory is introduced in this part to eliminate the conflict and achieve the CSA. The theory primarily comprises three elements, including discernment frame, basic probability assignment (BPA) function and combination rule [39].

Definition 3 (Discernment frame). A set Θ comprising independent, complete, and exclusive elements $\Phi_1, \Phi_2, \dots, \Phi_n$ is defined as a discernment frame. Its power set 2^Θ contains all possible subsets of the identification framework, which is written as follow:

$$2^\Theta = \{\emptyset, \{\Phi_1\}, \{\Phi_2\}, \dots, \{\Phi_n\}, \{\Phi_1 \cup \Phi_2\}, \{\Phi_1 \cup \Phi_3\}, \dots, \Theta\} \quad (4)$$

where \emptyset represents no obstacle is detected and $\{\Phi_1\}$ describes that obstacle Φ_1 is detected.

Definition 4 (Basic probability assignment). The basic probability assignment (BPA) is defined to better describe “uncertainty” and “unknown”. Assume that each obstacle Φ_i maps to a function $m(\Phi_i)$ ($m(\Phi_i) \in [0, 1]$). If $m(\Phi)$ satisfies

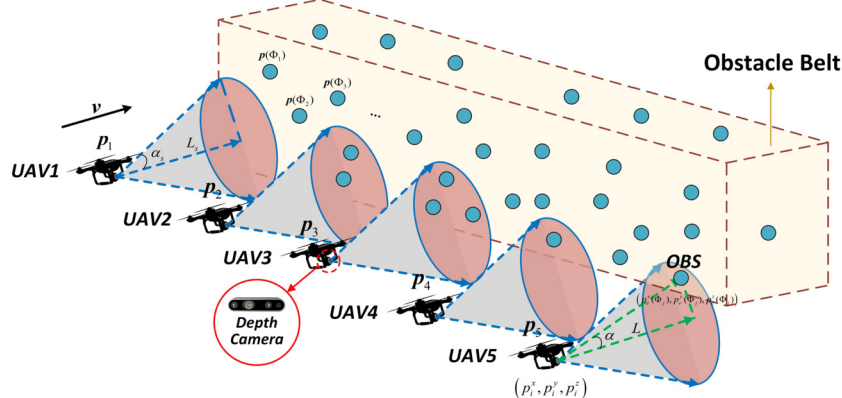


Fig. 4. Scenario assumption of multi-UAV detection.

$$m(\emptyset) = 0; m(\Phi) \geq 0; \sum_{\Phi=2^\Theta} m(\Phi) = 1, \quad (5)$$

then m is qualified as a BPA on Θ , where $m(\Phi)$ indicates the degree of support for evidence, excluding support for any true subset of Φ , and \emptyset refers to the empty set, which indicates that no obstacle is detected during the detection process.

Definition 5 (D-S combination rule). After determining the discernment frame, multiple independent sets of BPAs can be fused through the following D-S combination rule:

$$m(\Phi) = k \sum_{\substack{\Phi_1, \Phi_2, \dots, \Phi_n \subset \Theta \\ \Phi_1 \cap \Phi_2 \cap \dots \cap \Phi_n = \emptyset}} m_1(\Phi_1) m_2(\Phi_2) \dots m_n(\Phi_n), \quad (6)$$

for all $\Phi \subset \Theta, \Phi \neq \emptyset, \Phi_1, \Phi_2, \dots, \Phi_n \subset \Theta$, where k is the conflict coefficient, which can be expressed as

$$k = \left(1 - \sum_{\substack{\Phi_1, \Phi_2, \dots, \Phi_n \subset \Theta \\ \Phi_1 \cap \Phi_2 \cap \dots \cap \Phi_n = \emptyset}} m_1(\Phi_1) m_2(\Phi_2) \dots m_n(\Phi_n) \right)^{-1}. \quad (7)$$

Definition 6 (Belief and plausibility function). The upper and lower bounds of a probability interval are set in accordance with the mass assignments. The above interval covers the precise probability of an interest set (in the classical sense). It is associated with two non-additive continuous measures, including plausibility and belief (or support):

$$BEL(A) \leq P(A) \leq PL(A) \quad (8)$$

The belief $BEL(A)$ in terms of a set A represents the total masses of subsets of the interest set:

$$BEL(A) = \sum_{B|B \subseteq A} m(B) \quad (9)$$

The plausibility $PL(A)$ is the sum of all the masses of the sets B that intersect the interest set A :

$$PL(A) = \sum_{B|B \cap A \neq \emptyset} m(B) \quad (10)$$

The two measures are associated with each other in the following:

$$PL(A) = 1 - BEL(\bar{A}) \quad (11)$$

where \bar{A} denotes the complementary set of A .

2.4. Detection uncertainty

For depth camera, distortion occurs when it detects obstacles due to its inherent characteristics and the errors in manufacturing and assembly, leading to detection uncertainty. It is noteworthy that the detection accuracy decreases with the increase of the visual distance L . Additionally, the detection accuracy is affected by angular offset, that is, the accuracy decreases with the increase of the visual angle α . Thus, the detection accuracy is affected by both visual distances and angles.

Ref. [40] has suggested that the detection accuracy of two typical depth cameras, named Kinect v1 and structure sensor, decreases exponentially with the increase of the visual distance. Fig. 5 illustrates the data fitting result between detection accuracy and visual distance. Accordingly, their qualitative relationship is characterized with the exponential distribution, as shown in Fig. 6.

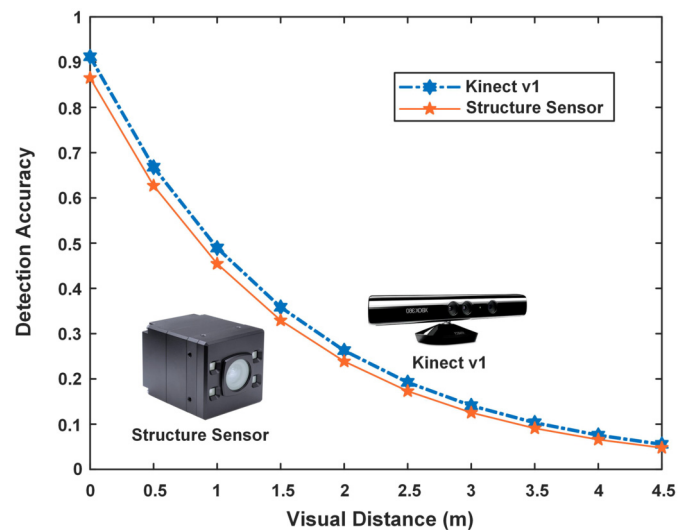


Fig. 5. Data fitting between detection accuracy and visual distance.

Additionally, the detection accuracy also indicates a specific distribution with the visual angle according to [41]. The fitting data curve is illustrated in Fig. 7. As shown in Fig. 7, the detection accuracy approximately presents a Gaussian distribution with visual distance on a certain distance. Thus, the qualitative relationship between detection accuracy of depth camera and visual distance is characterized with the Gaussian distribution, as depicted in Fig. 8.

Based on the analysis, we know that the detection accuracy approximately presents the exponential distribution with visual distance L and Gaussian distribution with visual angle α . Therefore, the exponential function $P(L)$ is adopted to describe the relationship between detection accuracy and visual distance, and the probability density function is defined as $f(L)$. The Gaussian distribution function $P(\alpha)$ is used to describe the relationship between detection accuracy and visual angle, and the probability density function is defined as $f(\alpha)$. They are mathematically expressed as

$$f(L) = \lambda e^{-\lambda L}, \quad f(\alpha) = \frac{1}{\sigma \sqrt{2\pi}} e^{\frac{-\alpha^2}{2\sigma^2}}, \quad (12)$$

where λ and σ represent the uncertainty coefficient of visual distance and angle, respectively.

Definition 7 (Detection accuracy). Combining Definition 2 and eliminating the effect of constant terms, the static detection accuracy is defined as

$$P_A(L, \alpha) = \sqrt{2\pi} \frac{\sigma}{\lambda} \cdot \frac{e^{-\frac{\alpha^2}{2\sigma^2}}}{\sigma \sqrt{2\pi}} \cdot \lambda e^{-\lambda L} \cdot \delta(L, \alpha) = e^{-\frac{\alpha^2}{2\sigma^2} - \lambda L} \cdot \delta(L, \alpha) \quad (13)$$

Note that $P_A(L, \alpha)$ is not a probability density function since it does not satisfy the basic properties. The purpose of this definition is to establish the BPA m . Taking time dimension into consideration, the BPA m in evidence theory is constructed as

$$\begin{aligned} m(L_t, \alpha_t) &= \sqrt{2\pi} \frac{\sigma}{\lambda} \cdot \frac{e^{-\frac{\alpha_t^2}{2\sigma^2}}}{\sigma \sqrt{2\pi}} \cdot \lambda e^{-\lambda L_t} \cdot \delta(L_t, \alpha_t) \\ &= e^{-\frac{\alpha_t^2}{2\sigma^2} - \lambda L_t} \cdot \delta(L_t, \alpha_t) \end{aligned} \quad (14)$$

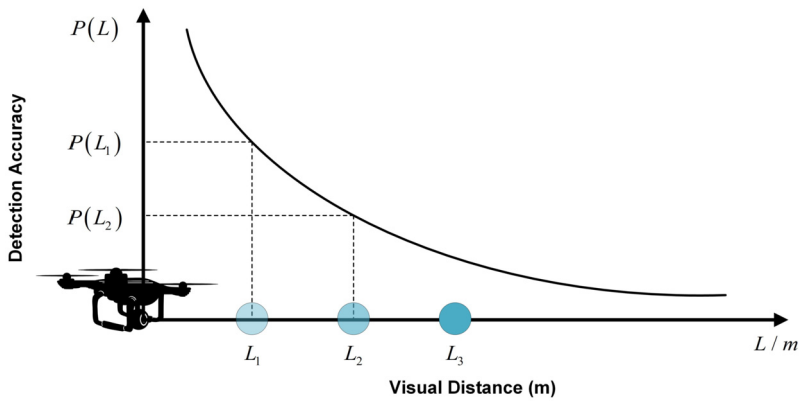


Fig. 6. Qualitative relationship between detection accuracy and visual distance.

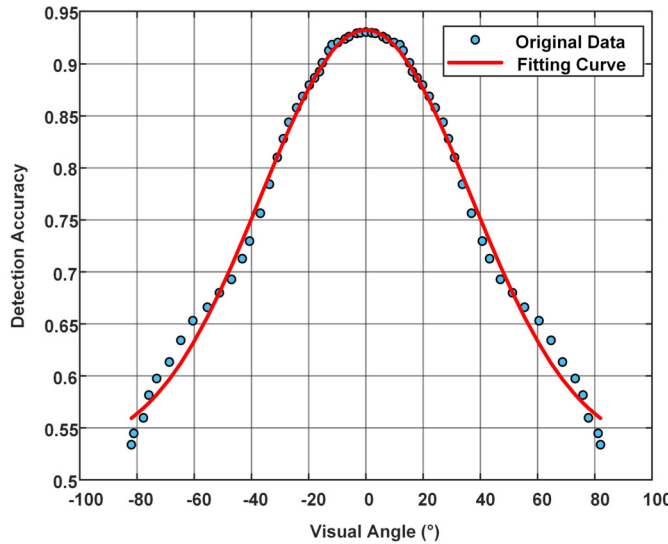


Fig. 7. Data fitting between detection accuracy and visual angle.

It can be verified that $m(L_t, \alpha_t)$ satisfies the conditions in (5), thus it can be qualified as the BPA. The visual angle α_t and the visual distance L_t at time t are given by

$$\begin{aligned} \alpha_t &= \arctan \frac{L_0 \tan \alpha_0}{L_0 - vt}, \\ L_t &= L_0 - vt, \end{aligned} \quad (15)$$

where α_0 is the visual angle when UAV detects obstacles at initial time and L_0 is the visual distance at initial time.

3. CSA based on improved D-S evidence theory

Notably, achieving CSA is challenging due to the randomness of obstacle distribution and detection uncertainties. In this section, an information fusion method is adopted by introducing and modifying the traditional D-S evidence theory, which is presented in Fig. 9. Firstly, the multi-UAV system detects and obtains the uncertain information about the obstacles, that is, the obstacle position in body-fixed coordinate frame $p_b(\Phi_j) = [p_b^x(\Phi_j), p_b^y(\Phi_j), p_b^z(\Phi_j)]^T$. Subsequently, the ground center transforms $p_b(\Phi)$ into $p_e(\Phi)$, fuses the information through D-S evidence theory, obtains the accurate fusion results $\mathbf{P}_{1,\dots,n}(\Phi)$ and disseminates them to the UAVs. Eventually, all UAVs receive the results and carry out follow-up decisions. It is worth mentioning that the CSA is conducted not only among multiple UAVs, but also among different times to achieve a higher detection accuracy.

3.1. CSA among multiple UAVs

We now apply the proposed fusion method into the CSA of the multi-UAV system. Without loss of generality, the information fusion among UAV I, II and III on OBS I is taken as an example. It is assumed that three UAVs detect an obstacle at time t_1 . The first step is to fuse information from all UAVs covering this obstacle. Fig. 10 illustrates this process. Additionally, it is worth mentioning that contradictory information may occur during the detection process. For example, UAV I detects the OBS I with high detection accuracy, while UAV II may report that it does not detect OBS I. This situation is called the trust paradox. Traditional D-S theory cannot deal with the problem and obtain accurate fusion results effectively. Thus, several trust paradoxes will be taken into consideration and discussed later.

As depicted in Fig. 10, the three UAVs detect and obtain the obstacle position $\mathbf{p}_i(\Phi_1)$ and corresponding BPAs $m_i(\Phi_1)$ ($i = 1, 2, 3$) initially, then information fusion is conducted for twice to obtain single-fusion results $m_{12}(\{\mathbf{p}_1(\Phi_1)\})$, $m_{12}(\{\mathbf{p}_2(\Phi_1)\})$, $m_{23}(\{\mathbf{p}_1(\Phi_1)\})$, $m_{23}(\{\mathbf{p}_2(\Phi_1)\})$, $\mathbf{P}_{12}(\Phi_1)$ and $\mathbf{P}_{23}(\Phi_1)$. Subsequently, we continue to fuse the data above and obtain the double-fusion results $m_{123}(\{\mathbf{p}_1(\Phi_1)\})$, $m_{123}(\{\mathbf{p}_2(\Phi_1)\})$, $m_{123}(\{\mathbf{p}_3(\Phi_1)\})$ and $\mathbf{p}_{123}(\Phi_1)$.

Based on Fig. 10, the BPAs and position information can be fused by

$$\mathbf{P}_{123}(\Phi_1) = \sum_{i=1}^3 \frac{m_{123}(\{\mathbf{p}_i(\Phi_1)\}) \cdot \mathbf{p}_i(\Phi_1)}{m_{123}(\{\mathbf{p}_i(\Phi_1)\})} \quad (16)$$

where $m_{123}(\{\mathbf{p}_1(\Phi_1)\})$, $m_{123}(\{\mathbf{p}_2(\Phi_1)\})$ and $m_{123}(\{\mathbf{p}_3(\Phi_1)\})$ refer to the BPAs, the physical meaning of which is the probability of OBS I at $\mathbf{p}_1(\Phi_1)$, $\mathbf{p}_2(\Phi_1)$ and $\mathbf{p}_3(\Phi_1)$, respectively, which are written as

$$\begin{aligned} m_{123}(\{\mathbf{p}_1(\Phi_1)\}) &= \frac{1}{k} \cdot \sum_{A \cap B \cap C = p_1(\Phi_1)} m_1(A)m_2(B)m_3(C) \\ &= \frac{1}{k} \cdot \{m_1(\Phi_1) \cdot [1 - m_2(\Phi_1)] \cdot [1 - m_3(\Phi_1)]\} \end{aligned} \quad (17)$$

$$\begin{aligned} m_{123}(\{\mathbf{p}_2(\Phi_1)\}) &= \frac{1}{k} \cdot \sum_{A \cap B \cap C = p_2(\Phi_1)} m_1(A)m_2(B)m_3(C) \\ &= \frac{1}{k} \cdot \{[1 - m_1(\Phi_1)] \cdot m_2(\Phi_1) \cdot [1 - m_3(\Phi_1)]\} \end{aligned} \quad (18)$$

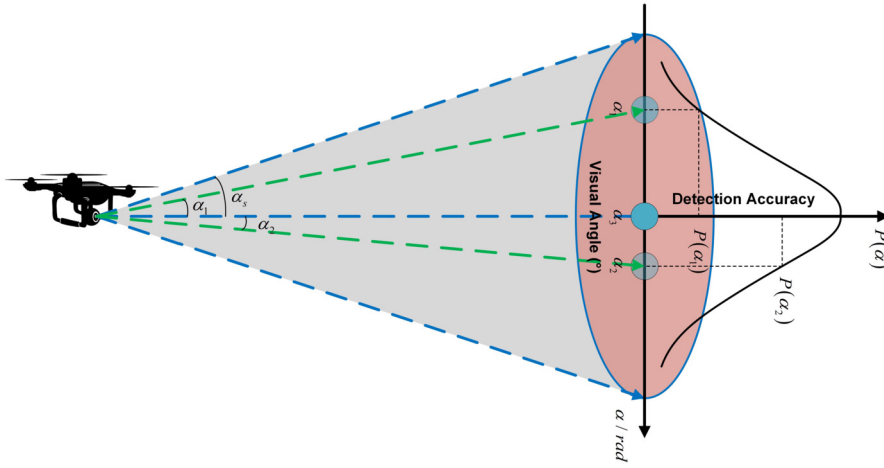


Fig. 8. Qualitative relationship between detection accuracy and visual angle.

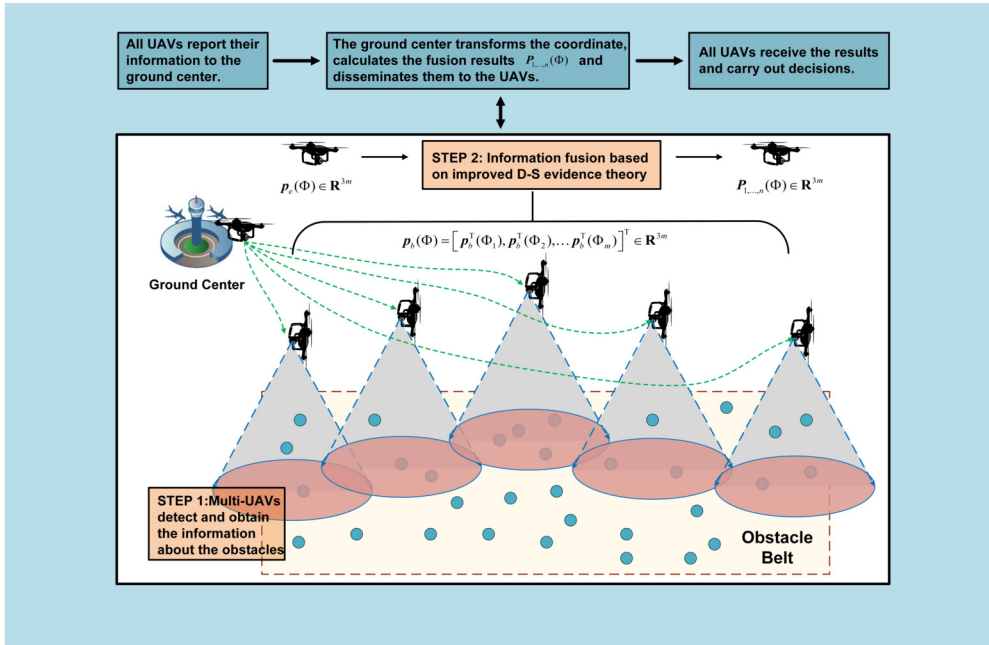


Fig. 9. Schematic diagram of the multi-UAV system CSA mission.

$$\begin{aligned} m_{123}(\{p_3(\Phi_1)\}) &= \frac{1}{k} \cdot \sum_{A \cap B \cap C = p_3(\Phi_1)} m_1(A)m_2(B)m_3(C) \\ &= \frac{1}{k} \cdot \{[1 - m_1(\Phi_1)] \cdot [1 - m_2(\Phi_1)] \cdot m_3(\Phi_1)\} \end{aligned} \quad (19)$$

where k is written as

$$\begin{aligned} k &= \sum_{A \cap B \cap C \neq \emptyset} m_1(A)m_2(B)m_3(C) \\ &= m_1(\Phi_1) \cdot [1 - m_2(\Phi_1)] \cdot [1 - m_3(\Phi_1)] \\ &\quad + [1 - m_1(\Phi_1)] \cdot m_2(\Phi_1) \cdot [1 - m_3(\Phi_1)] \\ &\quad + [1 - m_1(\Phi_1)] \cdot [1 - m_2(\Phi_1)] \cdot m_3(\Phi_1) \end{aligned} \quad (20)$$

On that basis, the BPA and coordinate information fusion results of UAV I, II and III on OBS I at time t_1 are yielded. Subsequently, the results are fused with the remaining UAVs, and the overall information fusion results of OBS I at time t_1 under the detection of all UAVs are achieved.

3.2. CSA among different times

Subsequently, the information fusion among different times is conducted to achieve the final CSA. Similarly, the information fusion among time t_1 , t_2 and t_3 on OBS I is selected as an example, which is illustrated in Fig. 11. Notably, time dimension is considered in this process, that is, the multi-UAV system flies forward and detects the obstacle belt under a fixed time step. Our task is to fuse the detection results under different times and obtain the CSA result. Moreover, similar trust paradoxes may also happen during this step since the detection results under different times can be highly contradictory too. The paradoxes will be considered and processed through the modifications of the traditional D-S evidence theory.

As shown in Fig. 11, the fusion results in the previous step are regarded as the original information of this step, that is, the fused obstacle position $p^{t_i}(\Phi_1)$ and corresponding BPAs $m^{t_i}(\Phi_1)$ ($i = 1, 2, 3$). Similarly, the obstacle position and BPAs are fused through

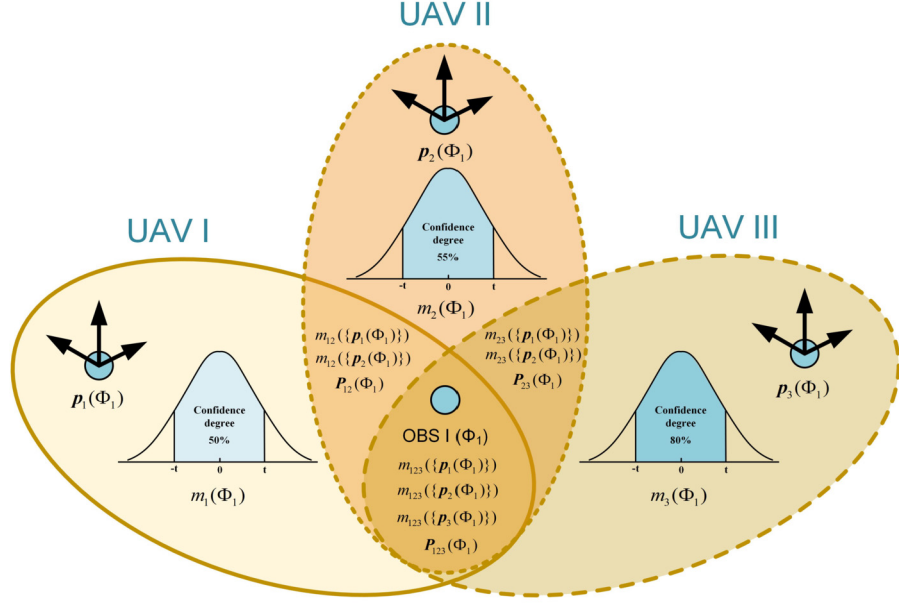


Fig. 10. Information fusion among multiple UAVs.

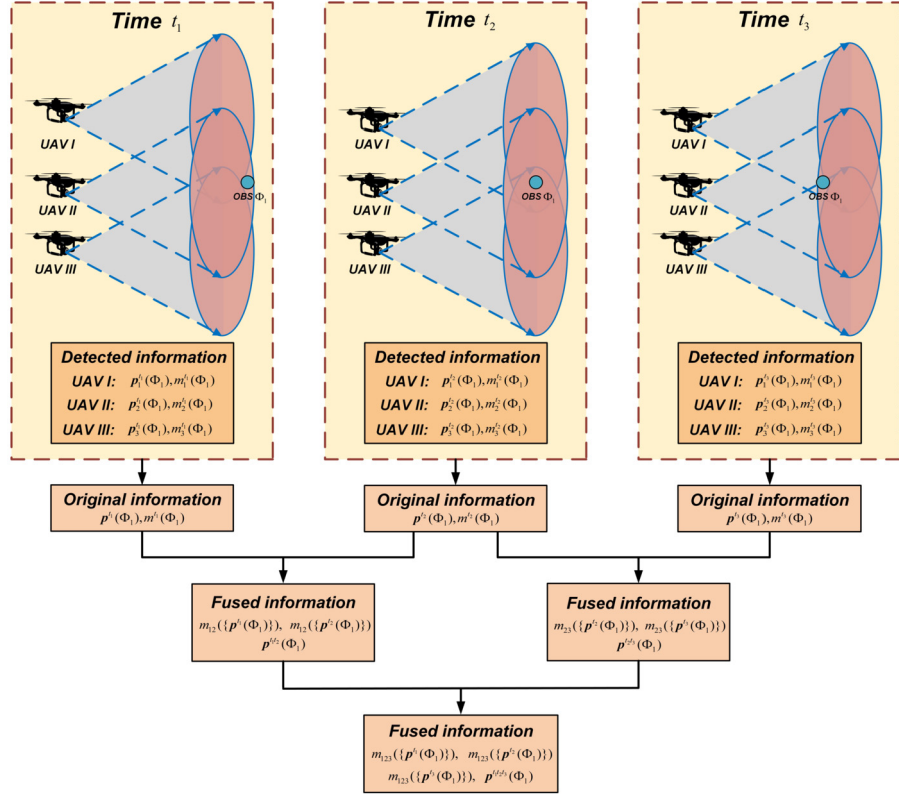


Fig. 11. Information fusion among different times.

$$\mathbf{P}^{t_1 t_2 t_3}(\Phi_1) = \sum_{i=1}^3 \frac{m^{t_1 t_2 t_3}(\{\mathbf{p}^{t_i}(\Phi_1)\}) \cdot \mathbf{p}^{t_i}(\Phi_1)}{m^{t_1 t_2 t_3}(\{\mathbf{p}^{t_i}(\Phi_1)\})} \quad (21)$$

The calculation of $m^{t_1 t_2 t_3}(\{\mathbf{p}^{t_i}(\Phi_1)\})$ ($i = 1, 2, 3$) and conflict coefficient k are similar with Section 3.1, which are mathematically expressed as

$$\begin{aligned} m^{t_1 t_2 t_3}(\{\mathbf{p}^{t_1}(\Phi_1)\}) \\ = \frac{1}{k} \cdot \sum_{A \cap B \cap C = \mathbf{p}^{t_1}(\Phi_1)} m_1(A)m_2(B)m_3(C) \end{aligned}$$

$$= \frac{1}{k} \cdot \{m^{t_1}(\Phi_1) \cdot [1 - m^{t_2}(\Phi_1)] \cdot [1 - m^{t_3}(\Phi_1)]\} \quad (22)$$

$$\begin{aligned} m^{t_1 t_2 t_3}(\{\mathbf{p}^{t_2}(\Phi_1)\}) \\ = \frac{1}{k} \cdot \sum_{A \cap B \cap C = \mathbf{p}^{t_2}(\Phi_1)} m_1(A)m_2(B)m_3(C) \end{aligned}$$

$$\begin{aligned} m^{t_1 t_2 t_3}(\{\mathbf{p}^{t_3}(\Phi_1)\}) \\ = \frac{1}{k} \cdot \{[1 - m^{t_1}(\Phi_1)] \cdot m^{t_2}(\Phi_1) \cdot [1 - m^{t_3}(\Phi_1)]\} \end{aligned} \quad (23)$$

Table 1
BPA of four pieces of common conflict evidence.

Paradoxes	Evidence	Propositions				
		A	B	C	D	E
Complete conflict paradox (1)	m_1	1	0	0	\	\
	m_2	0	1	0	\	\
	m_3	0.8	0.1	0.1	\	\
	m_4	0.8	0.1	0.1	\	\
0 trust paradox (2)	m_1	0.5	0.2	0.3	\	\
	m_2	0.5	0.2	0.3	\	\
	m_3	0	0.9	0.1	\	\
	m_4	0.5	0.2	0.3	\	\
1 trust paradox (3)	m_1	0.9	0.1	0	\	\
	m_2	0	0.1	0.9	\	\
	m_3	0.1	0.15	0.75	\	\
	m_4	0.1	0.15	0.75	\	\
High conflict paradox (4)	m_1	0.7	0.1	0.1	0	0.1
	m_2	0	0.5	0.2	0.1	0.2
	m_3	0.6	0.1	0.15	0	0.15
	m_4	0.55	0.1	0.1	0.15	0.1
	m_5	0.6	0.1	0.2	0	0.1

Table 2
Fusion results of conflict evidence using the D-S evidence theory.

Paradoxes	k	BPA of propositions after fusion					D-S	Convention
		A	B	C	D	E		
(1)	1	\	\	\	\	\		A
(2)	0.99	0	0.727	0.273	\	\	B	A
(3)	0.9998	0	1	0	\	\	B	C
(4)	0.9999	0	0.3571	0.4286	0	0.2143	C	A

$$\begin{aligned}
 &= \frac{1}{k} \cdot \sum_{A \cap B \cap C = p^{t_3}(\Phi_1)} m_1(A)m_2(B)m_3(C) \\
 &= \frac{1}{k} \cdot \{ [1 - m^{t_1}(\Phi_1)] \cdot [1 - m^{t_2}(\Phi_1)] \cdot m^{t_3}(\Phi_1) \} \quad (24)
 \end{aligned}$$

$$\begin{aligned}
 k &= \sum_{A \cap B \cap C \neq \emptyset} m_1(A)m_2(B)m_3(C) \\
 &= m^{t_1}(\Phi_1) [1 - m^{t_2}(\Phi_1)] [1 - m^{t_3}(\Phi_1)] \\
 &\quad + [1 - m^{t_1}(\Phi_1)] m^{t_2}(\Phi_1) [1 - m^{t_3}(\Phi_1)] \\
 &\quad + [1 - m^{t_1}(\Phi_1)] [1 - m^{t_2}(\Phi_1)] m^{t_3}(\Phi_1) \quad (25)
 \end{aligned}$$

Through this step, the BPAs and coordinate information fusion results of all times on OBS I are obtained. Afterwards, the results are fused with the subsequent moments, and the overall information fusion results of Obstacle I under the detection of all UAVs at all times can be obtained to yield the final result of CSA.

3.3. Defects of the conventional D-S evidence theory

Conventional D-S evidence theory is capable of dealing with the uncertainties in CSA to a certain degree, whereas it still has limitations in processing evidence with complete or high conflict. A complete conflict example is presented as follows to illustrate the limitations.

It is assumed that two UAVs detect an obstacle and obtain its position p_1 and p_2 , respectively. Thus, the discernment frame can be expressed by $\Theta = \{p_1, p_2\}$, and the detection results of the two UAVs are written as

$$\begin{aligned}
 \text{UAV I: } m_1(p_1) &= 0, m_1(p_2) = 1; \\
 \text{UAV II: } m_2(p_1) &= 1, m_2(p_2) = 0. \quad (26)
 \end{aligned}$$

Conflict coefficient $k = 1$ is obtained through calculation, thus suggesting that two sources of evidences are of complete conflict.

Besides, the numerator is zero in accordance with the combination rule in Eq. (5), thus suggesting that the formula is invalid, and that information fusion cannot be achieved.

For evidence with high conflict, the fusion results of D-S evidence theory also often violate common sense. Table 1 presents BPAs of four pieces of common conflict evidence, and Table 2 presents the fusion results.

- (1) **Complete conflict paradox:** the example above has explained that conventional D-S evidence theory is invalid when $k = 1$.
- (2) **0 trust paradox:** the conflict coefficient can be calculated as $k = 0.99$. It can be checked that because evidence m_3 totally denies proposition A , the BPA for proposition A in the synthesis results will always be zero no matter how strongly evidence m_1 , m_2 and m_4 support proposition A . That is, D-S combination rule has the disadvantage of one ballot veto.
- (3) **1 trust paradox:** the conflict coefficient can be calculated as $k = 0.9998$. Although all sources of evidence give small BPAs to proposition B , the synthesis results completely believe proposition B is the correct proposition, which is per-verse in practical application.
- (4) **High conflict paradox:** the total conflict factor can be calculated as $k = 0.9999$. It can be proved in a similar way that precise synthesis results should support proposition A as evidence m_1 , m_3 , m_4 and m_5 all give proposition A large BPAs. However, high conflicts in the above evidence cause erroneous reasoning.

Since the combination of conventional D-S evidence often fails due to the particularity of some propositions and the existence of conflicting propositions, scholars have developed several improved methods from the perspective of modifying the source of evidence, the core of which are to redistribute the weight of each evidence according to their relevance and conflict. Nevertheless, most of them ignored the significance of BPA in the original propositions.

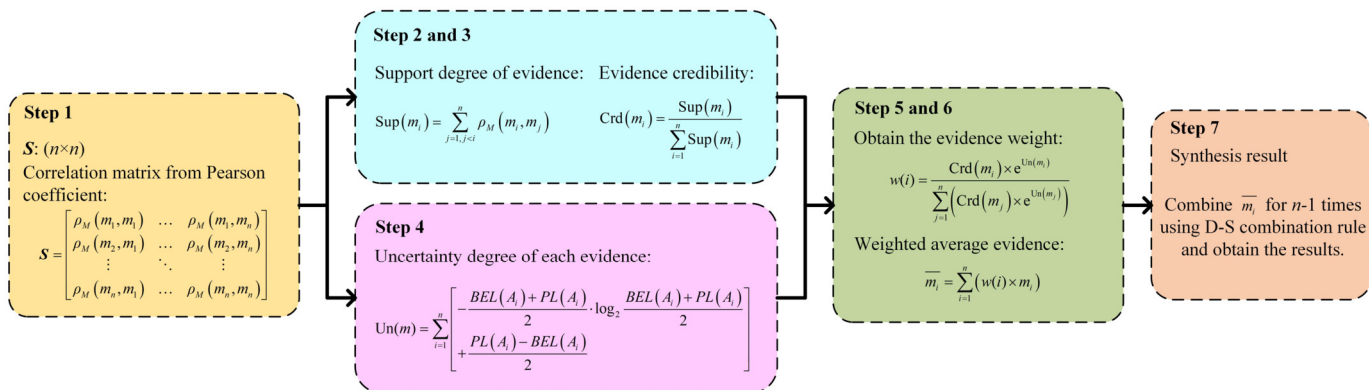


Fig. 12. The flow chart of improved evidence combination method.

Thus, we analyze and improve the BPA of the original evidence, and then adopt the D-S combination rule to ensure the integrity of the improved D-S evidence theory.

3.4. Improved information fusion method towards high conflict evidence

3.4.1. Similarity measure based on Pearson correlation coefficient

Denote m_1 and m_2 as two evidence bodies based on the discernment frame Θ . Then the correlation between the two pieces of evidence can be calculated according to

$$\rho_{12} = \frac{\text{cov}(m_1, m_2)}{\sigma_{m_1} \sigma_{m_2}} = \frac{E((m_1 - \mu_{m_1})(m_2 - \mu_{m_2}))}{\sigma_{m_1} \sigma_{m_2}} \quad (27)$$

where ρ_{12} refers to the Pearson coefficient between m_1 and m_2 , $\text{cov}(m_1, m_2)$ indicates the covariance between two pieces of evidence, $E(m_i)$ denotes the mathematical expectation of m_i ; μ_{m_i} and σ_{m_i} are mathematically expressed by

$$\begin{aligned} \mu_{m_i} &= E(m_i) \\ \sigma_{m_i}^2 &= E((m_i - E(m_i))^2) \\ &= E(m_i^2) - E^2(m_i). \end{aligned} \quad (28)$$

The range of Pearson coefficient is $[-1, 1]$. Negative values indicate negative correlation, and smaller negative values mean higher negative correlation. Moreover, the Pearson coefficient less than zero is modified as zero in order to satisfy the non-negative condition of correlation coefficient as well as to reduce the effect of negative value on basic probability. Therefore, the modified Pearson coefficient $\rho_M(m_i, m_j)$ between m_i and m_j can be described by

$$\rho_M(m_i, m_j) = \begin{cases} \rho_{ij}, & \text{if } \rho_{ij} \geq 0, \\ 0, & \text{otherwise.} \end{cases} \quad (29)$$

Lemma 1. The following properties are satisfied for $\rho_M(m_i, m_j)$.

- 1) $0 \leq \rho_M(m_i, m_j) \leq 1$.
- 2) $\rho_M(m_i, m_j) = \rho_M(m_j, m_i)$.
- 3) $\rho_M(m_i, m_j) = 1 \Leftrightarrow m_j = am_i + b$, where a and b are constants.

Proof. The proof of Lemma 1 is reported in Appendix A. ■

3.4.2. Uncertainty measure based on evidence interval probability

The method in Section 3.4.1 only considers the correlation between the evidence and evaluates the evidence from merely one

perspective, which is not comprehensive enough. On that basis, evidence uncertainty is introduced, and conflicting evidence is modified in different aspects.

Evidence theory suggests that the confidence interval $[BEL(\Phi), PL(\Phi)]$ can be determined in accordance with BPA, and the interval confidence of all single-element subsets can be considered as the interval probability. For BPA based on the discernment frame $\Theta = \{\Phi_1, \Phi_2, \dots, \Phi_n\}$, all the confidence intervals constitute the interval probability distribution on Θ . Moreover, the uncertainty of interval probability (e.g., the uncertainty of evidence) comprises inconsistency and imprecision. Thus, confidence interval is employed for qualification. The median value $\frac{PL(\Phi_i) + BEL(\Phi_i)}{2}$ of all interval probabilities is employed to obtain the inconsistency, and the interval length $PL(\Phi_i) + BEL(\Phi_i)$ is used to obtain the inaccuracy. Based on this idea, a novel uncertainty measure is introduced.

For each given evidence bodies, we are able to obtain their belief BEL and plausibility PL through Eq. (9) and (10). Then the uncertainty degree $Un(m)$ of BPA m can be mathematically expressed by

$$\begin{aligned} Un(m) = \sum_{i=1}^n & \left[-\frac{BEL(\Phi_i) + PL(\Phi_i)}{2} \right. \\ & \cdot \log_2 \frac{BEL(\Phi_i) + PL(\Phi_i)}{2} + \frac{PL(\Phi_i) - BEL(\Phi_i)}{2} \left. \right] \end{aligned} \quad (30)$$

3.4.3. A novel evidence weight assignment method

In this study, the Pearson coefficient is adopted to build the correlation measure between different pieces of evidence and determines the evidence credibility, whereas evidence uncertainty is considered comprehensively. The result of the analysis suggests that evidence credibility represents the degree of its support by other evidences, and evidence uncertainty represents the degree of conflict between it and other evidences. Thus, the weight of the evidence with high credibility should be increased and the weight of the evidence with high uncertainty should be reduced during the evidence combination. Accordingly, this study combines the credibility and uncertainty to determine the weight coefficient of the evidence, revise the original evidence, weighted average the BPA of the revised evidence, and then use the D-S combination rule to fuse it, so as to solve the evidence conflict. The flow chart of the improved method is illustrated in Fig. 12.

- 1) Calculate the modified Pearson coefficient $\rho_M(m_i, m_j)$ between two evidences and establish the correlation matrix S :

Table 3
Simulation parameters setting.

Item	Parameter	Item	Parameter
Obstacle space	300 m × 200 m × 100 m	Δt	1 s
n_{OBS}	From 20 to 100	λ	0.6
n_{UAV}	5	σ	1
$v_i = [v_i^x, v_i^y, v_i^z]^T$	[20, 0, 0]^T m/s	L_s	0 ~ 550 m
Velocity direction	Positive X axis	θ_s	-45° ~ +45°

$$\mathbf{S} = \begin{bmatrix} \rho_M(m_1, m_1) & \dots & \rho_M(m_1, m_n) \\ \rho_M(m_2, m_1) & \dots & \rho_M(m_2, m_n) \\ \vdots & \ddots & \vdots \\ \rho_M(m_n, m_1) & \dots & \rho_M(m_n, m_n) \end{bmatrix} \quad (31)$$

2) Calculate the support degree $Sup(m_i)$ of evidence m_i . Note that $Sup(m_i)$ may be zero due to high evidence conflict. As a result, the denominator will be zero too in step 3) and subsequent calculation. Thus, we modify and assign $Sup(m_i)$ to a small number ϵ ($\epsilon = 0.001$ in this study) if it is zero.

$$Sup(m_i) = \sum_{j=1, j < i}^n \rho_M(m_i, m_j) \quad (32)$$

3) Calculate the credibility $Crd(m_i)$ through

$$Crd(m_i) = \frac{Sup(m_i)}{\sum_{i=1}^n Sup(m_i)} \quad (33)$$

4) Calculate the uncertainty degree $Un(m_i)$ of each evidence according to Eq. (30).

5) Obtain the weight according to evidence credibility $Crd(m_i)$ and uncertainty $Un(m_i)$. Denote $w(i)$ as the weight of evidence, then it can be calculated by

$$w(i) = \frac{Crd(m_i) \times e^{Un(m_i)}}{\sum_{j=1}^n (Crd(m_j) \times e^{Un(m_j)})} \quad (34)$$

6) Weighted average the original evidence using the normalized weight coefficient and obtain the modified evidence \bar{m}_i by

$$\bar{m}_i = \sum_{i=1}^n (w(i) \times m_i) \quad (35)$$

7) Combine the weighted average evidence \bar{m}_i for $n - 1$ times using the D-S combination rule and obtain the results.

4. Case study

In this section, we give three simulation cases and corresponding analyses. The first case is the comparison between our CSA scheme of the multi-UAV system and SA of a single UAV, which verifies the feasibility of the method. The second case is the application of the CSA method under flexible formation shapes, which demonstrate the scalability and universality of the method in practice. The third case is the comparison of performances between the modified algorithm and four existing methods, which validates the superiority of our method. The simulations are conducted with MATLAB software on Windows 10 system, while the obstacles are randomly distributed in a given 3D space using the Monte Carlo stochastic modeling method. The average time of simulation is 3.284 s, and the simulation parameters are set as Table 3.

4.1. Comparison between the CSA of the multi-UAV system and SA of a single UAV

The CSA of the multi-UAV system under a specific formation shape is conducted first. The purpose of this case study is to verify

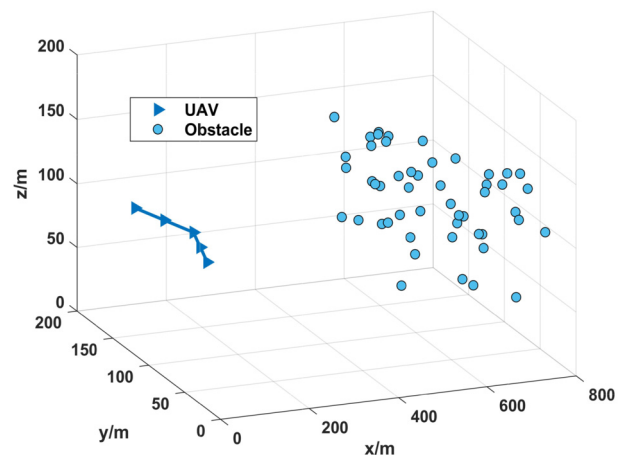


Fig. 13. Distribution of UAVs and obstacles under a certain formation shape.

Table 4
Quantitative comparison results between SA of a single UAV and CSA.

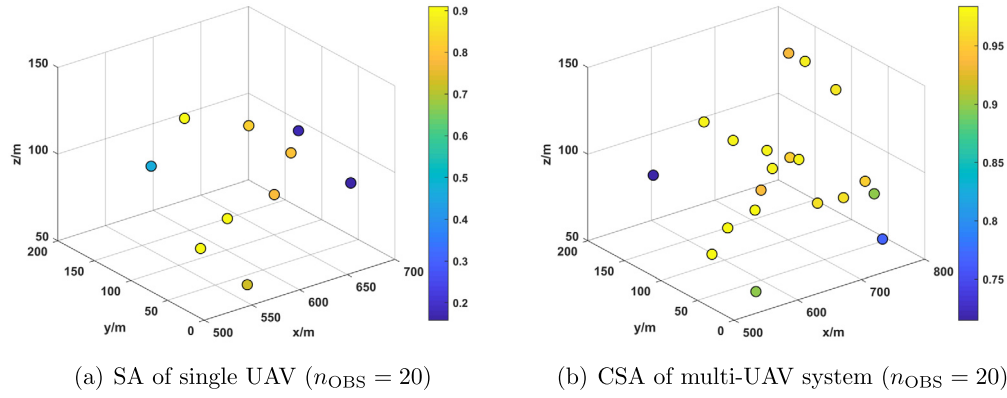
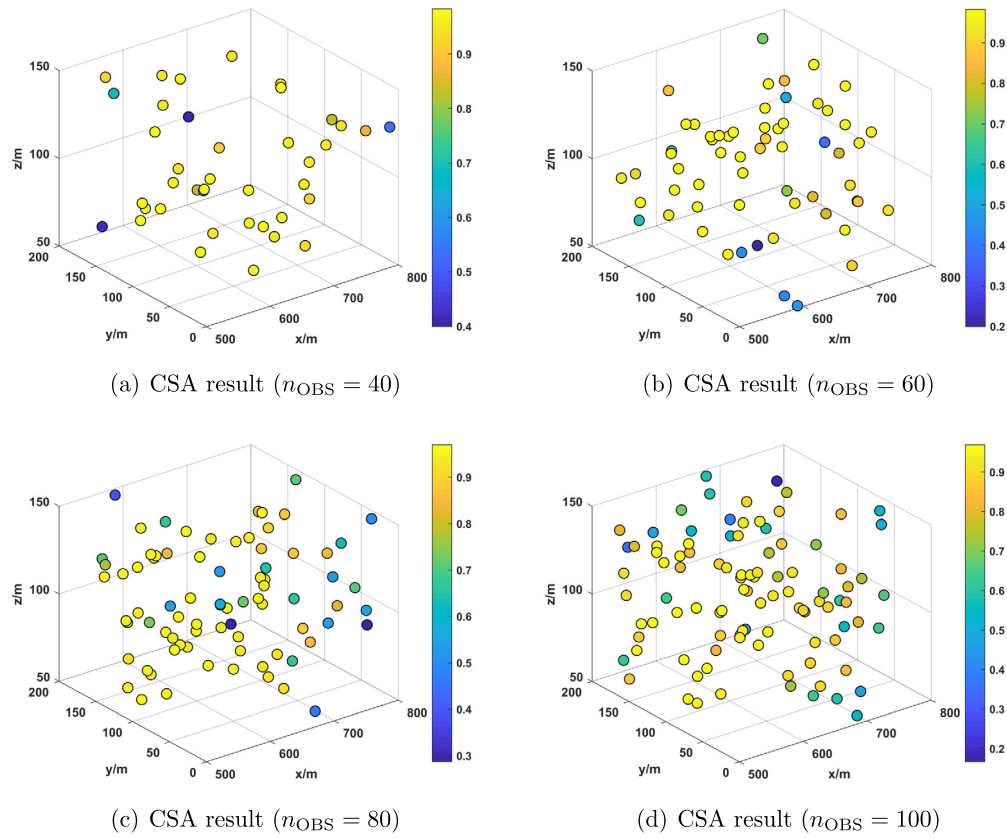
n_{OBS}	Method	Detected obstacles	Average detection accuracy
20	SA	10	33.18%
	CSA	20	93.85%
40	SA	23	41.25%
	CSA	40	90.87%
60	SA	38	39.47%
	CSA	60	87.33%
80	SA	42	32.41%
	CSA	79	82.66%
100	SA	39	17.52%
	CSA	98	79.09%

that a multi-UAV system can detect obstacles more widely and accurately using our developed CSA method, compared with SA of a single UAV. The distribution of multi-UAV system and obstacles is shown in Fig. 13. Note that the formation shape (called Formation I) is fixed, while the number and distribution of obstacles are both different in each test.

The comparison between the SA of a single UAV and CSA of the multi-UAV system is illustrated in Fig. 14(a) and Fig. 14(b). Note that the circles are obstacles, while shades of color represent the degree of detection accuracy. Besides, the number of obstacles n_{OBS} is set as 20.

Fig. 14(a) depicts the SA result of a single UAV for a single sampling time, which shows that only a few obstacles are detected, whereas the detection accuracy is generally low. As depicted in Fig. 14(b), the improved CSA method of the multi-UAV system can significantly detect more obstacles while being aware of the obstacles more accurately, with an average detection accuracy above 90%. Next, we extend the number of obstacles n_{OBS} to 40, 60, 80 and 100, respectively and obtain the CSA result of the multi-UAV system in Fig. 15 and Table 4.

According to the CSA results illustrated in Fig. 15 and quantitative comparison results expressed in Table 4, our CSA scheme can improve both the quantity and quality of obstacle detection. Compared with SA of a single UAV, the CSA of the multi-UAV system can detect twice the number of obstacles, and the average detection accuracy is also 40% ~ 50% higher. Even when n_{OBS} increases to 100, our scheme can still detect most obstacles and maintain the average detection accuracy at about 80%. Possible reasons include that the proposed CSA scheme has a wider detection range and can improve detection accuracy through information interaction and fusion. The results validate the effectiveness and superiority of the proposed CSA method.

**Fig. 14.** Comparison of detection accuracy between SA of a single UAV and CSA.**Fig. 15.** CSA results of the multi-UAV system with different obstacle numbers.

4.2. CSA under flexible formation shapes

In this section, the CSA results are extended for multiple times of sampling and the dynamic variation of detection accuracy is evaluated. Furthermore, to verify the scalability of the developed method, we fix the obstacle number n_{OBS} (the obstacle distribution is still random) and apply five formation shapes into the multi-UAV system, as shown in Fig. 16.

Additionally, to better illustrate the dynamic process of the multi-UAV system detecting obstacles, we divide the obstacle region into three parts, as shown in Fig. 17. The regions covered by red solid line, black dotted line and blue dashed line are accordingly the Area I, II and III. It is worth noting that the five formations are drawn on different planes in order to be distinguished, while they remain on the same plane during the simulation. Same as the above setting, all the multi-UAV systems fly forward at a

constant speed of 20 m/s along the X-axis. The detection accuracy of the three areas is illustrated in Fig. 18.

As depicted in Fig. 18, after multiple fusions, all formations can complete the detection in the three areas with high detection accuracy, whereas Formation I achieves a maximum detection accuracy of 96.58% in Area I. Such an improvement is due to more sparse distribution, wider detection range and no mutual obstruction of view.

Note that the trends in detection accuracy in the three areas are not consistent. In Area I, the detection accuracy of all formations increases rapidly with the increase in sampling times. However, in Area II, the detection accuracy of Formations III, IV, and V oscillates slightly at first and increases gradually after the third sampling time. In Area III, all formations start to detect obstacles after the fourth sampling time. Afterwards, the detection accuracy of all formations oscillates locally but shows an overall increasing trend.

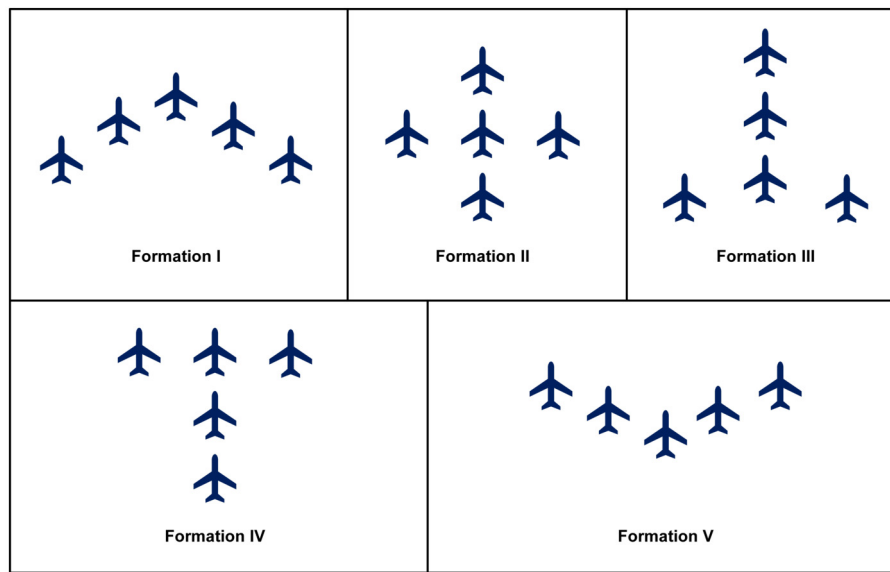


Fig. 16. Five formation shapes.

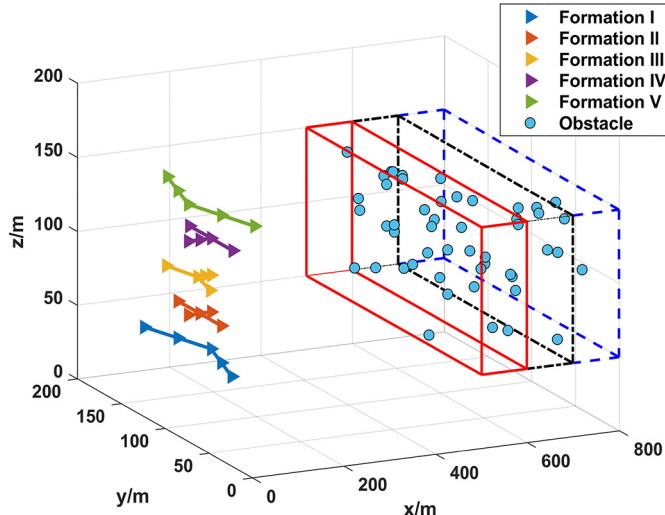


Fig. 17. Distribution of UAVs and obstacles under flexible formations.

Possible reason includes the relative distance between the obstacle area and the multi-UAV system. Area I is closest to the multi-UAV system and may already be within the detection range of the depth camera, while the obstacles in Area III may not be detected during the first few sampling times. In addition, Formation I has the widest overall detection range, and the view of each UAV in the system is not obscured by other UAVs. Thus, the detection accuracy of Formation I shows a distinguishing increase among the five formations.

It is worth mentioning that all formations can finally maintain a relatively high detection accuracy (above 80%) after our CSA scheme is applied, which validates the effectiveness and scalability of the proposed method.

4.3. Comparison between the improved algorithm and existent methods

The advantages of the improved method in this study are verified under the given recognition framework and evidence. We take four paradoxes described in Section 3.3 as examples to discuss the rationality and validity of the modified algorithm. The BPAs of four common paradoxes are illustrated in Fig. 19.

Fig. 19 suggests that evidence during the CSA process can be divided into consistent evidence and conflicting evidence. Apparently, the relatively consistent evidence includes m_1 , m_3 , and m_4 in complete conflict paradoxes, m_1 , m_2 , and m_4 in 0 trust paradox, m_2 , m_3 , and m_4 in 1 trust paradox, and m_1 , m_3 , m_4 and m_5 in high conflict paradox. Thus, accurate synthesis results should agree with the above consistent evidence while being away from conflicting evidence.

Notably, the conventional D-S combination rule cannot manage all four paradoxes. In this study, four existing improved methods developed by Yager [33], Sun et al. [34], Murphy [35], and Li et al. [37] (called Yager, Sun, Murphy, and Li for short) are selected for comprehensive analyses with the improved method (called Improved for short). The synthesis results are presented in Table 5 and Fig. 20. According to the results, the following discussions are conducted.

- (1) **Complete conflict paradox:** m_1 , m_3 , and m_4 are the relatively consistent evidence. Yager gives the uncertain domain Θ the whole belief as $m(\Theta) = 1$, which, on the contrary, increases propositions' uncertainty. Sun only solves part of the conflicts as the BPAs of propositions A, B, and C match the BPAs' proportion of the above consistent evidence, whereas the BPA for Θ remains high as $m(\Theta) = 1$, which still has high uncertainty. Furthermore, Murphy, Li, and Improved get relatively accurate results for complete conflict paradoxes.
- (2) **0 trust paradox:** m_1 , m_2 , and m_4 are the relatively consistent evidence. It is easy to check that the consistent evidence is the same, such that the most valid algorithm should have the minimum difference between the synthesis results and the consistent evidence. As can be seen intuitively, Yager presents totally wrong results, and Improved is the most effective algorithm in this kind of paradox.
- (3) **1 trust paradox:** m_2 , m_3 , and m_4 are the relatively consistent evidence. Yager and Sun cannot solve this paradox practically, which can be demonstrated in a similar way to the discussion of Case (1). Furthermore, Murphy, Li, and Improved are capable of managing 1 trust paradox to different degrees.
- (4) **High conflict paradox:** m_1 , m_3 , m_4 , and m_5 are the relatively consistent evidence. Yager and Sun are logical theoretically but cannot be put into practice because of their increasing uncertainty. Murphy, Li, and Improved all produce relatively reasonable results in this kind of paradox.

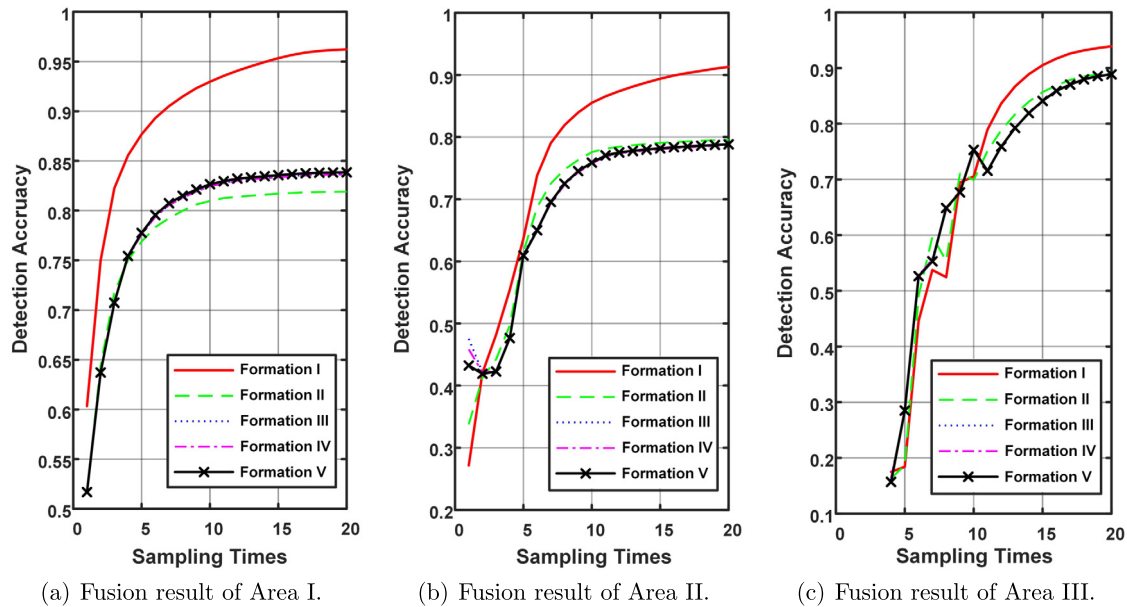


Fig. 18. Fusion results of the three areas.

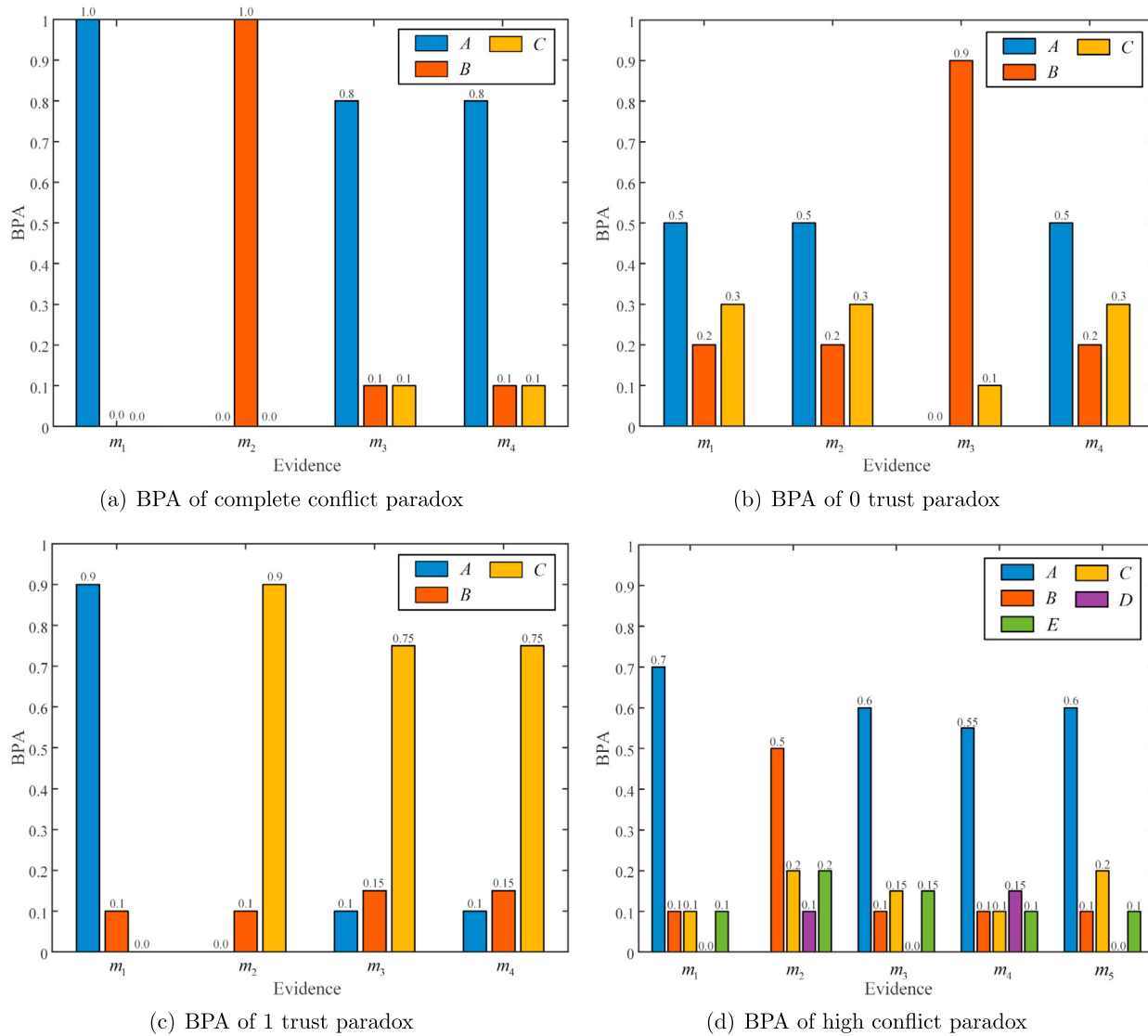
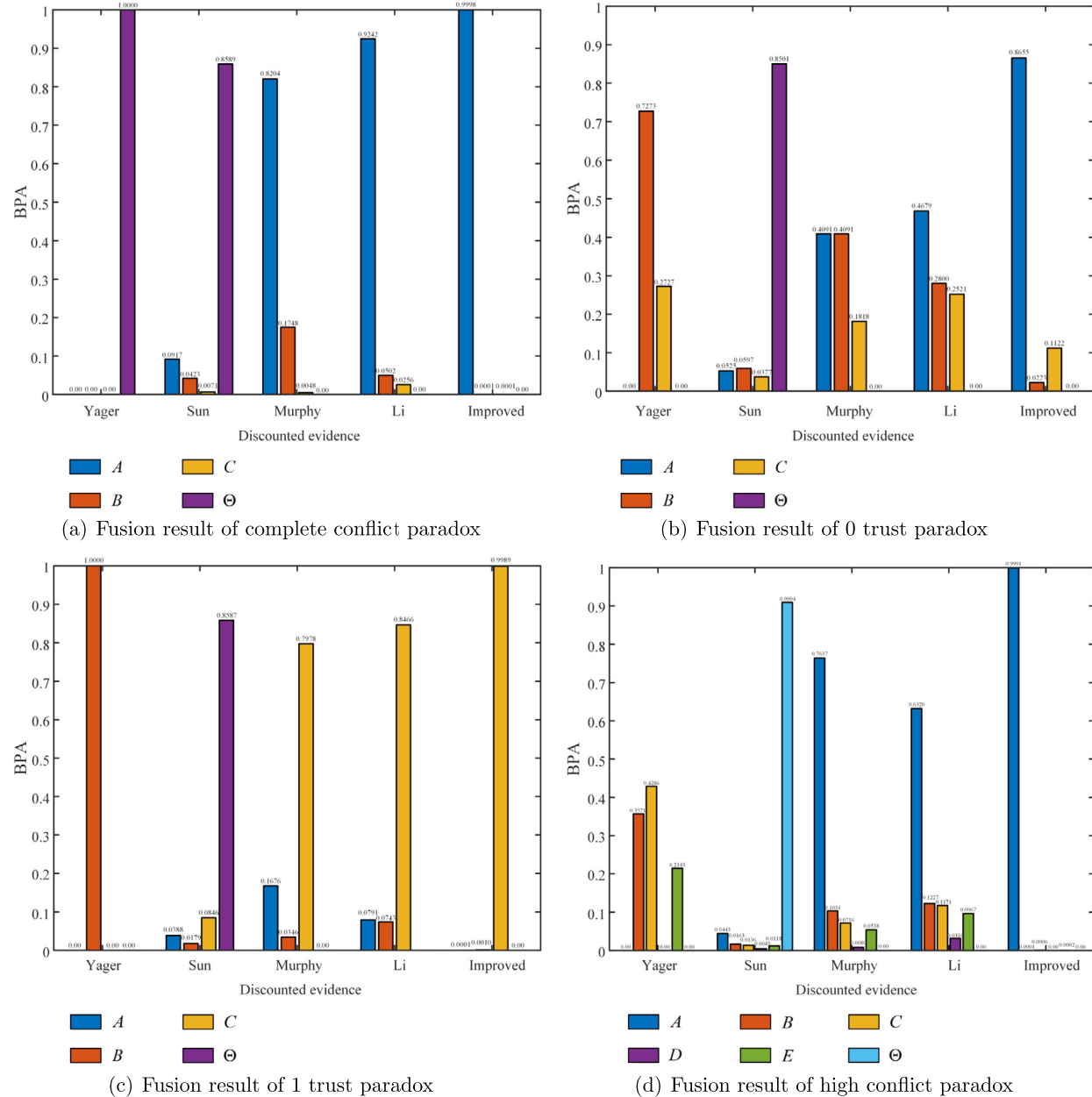


Fig. 19. BPAs of four common paradoxes.

**Fig. 20.** Comparison of the fusion results.

The propositions with four kinds of evidence conflicts in Table 5 should be AAC. The fusion results using the developed method can identify the corresponding propositions with the maximum BPAs. The results are consistent with common sense and are valid for all four kinds of conflicts. Moreover, it can be confirmed that *Yager* will generate incorrect results of synthesis based on paradoxes, and it is unable to handle any kind of paradox. *Sun* allocates most of the conflicts directly to Θ , which only solves paradoxes theoretically. It is not suitable for practical application because of the increasing uncertainty of synthesis results. *Murphy* averages all evidence without separating consistent evidence and conflicting evidence. Besides, it is not capable of solving paradoxes since evidence has an inconsistent contribution to the results of synthesis, regardless of its simple computation. Thus, only *Li* and *Improved* can generate relatively reasonable synthesis results for all the above four common paradoxes. Besides, by comparing the BPA obtained by the algorithm in Table 5, we obtain that the *Improved* algorithm has the highest identification BPA for reasonable

propositions, which proves that our method performs better than all other algorithms in solving the four conflicts above.

5. Conclusion and future work

Based on the background of UAV detection, this study applies the improved D-S evidence theory to the CSA of the multi-UAV system to conduct the information fusion detected by airborne sensors, which demonstrates superior performance on dealing with detection uncertainty. Compared to the SA of a single UAV, the proposed CSA scheme for the multi-UAV system is able to detect more obstacles and perceive the obstacles more accurately, with a 40% ~ 50% higher average detection accuracy. In the case study of CSA under flexible formation shapes, the detection accuracy under different formation shapes is illustrated by a diagram of curves. The uncertainty of fusion results decreases, and the accuracy increases as more pieces of information are fused. Additionally, compared to existing methods based on the modified D-S evidence

Table 5
Comparison of the combination results.

Paradoxes	Methods	Propositions					
		A	B	C	D	E	F
(1)	<i>Yager</i>	0	0	0	\	\	1
	<i>Sun</i>	0.0917	0.0423	0.0071	\	\	0.8589
	<i>Murphy</i>	0.8204	0.1748	0.0048	\	\	0
	<i>Li</i>	0.9242	0.0502	0.0256	\	\	0
(2)	Improved	0.9998	0.0001	0.0001	\	\	0
	<i>Yager</i>	0	0.7273	0.2727	\	\	0
	<i>Sun</i>	0.0525	0.0597	0.0377	\	\	0.8501
	<i>Murphy</i>	0.4091	0.4091	0.1818	\	\	0
	<i>Li</i>	0.4679	0.2800	0.2521	\	\	0
(3)	Improved	0.8655	0.0223	0.1122	\	\	0
	<i>Yager</i>	0	1	0	\	\	0
	<i>Sun</i>	0.0388	0.0179	0.0846	\	\	0.8587
	<i>Murphy</i>	0.1676	0.0346	0.7978	\	\	0
(4)	<i>Li</i>	0.0791	0.0743	0.8466	\	\	0
	Improved	0.0001	0.0010	0.9989	\	\	0
	<i>Yager</i>	0	0.3571	0.4286	0	0.2143	0
	<i>Sun</i>	0.0443	0.0163	0.0136	0.0045	0.0118	0.9094
(5)	<i>Murphy</i>	0.7637	0.1031	0.0716	0.0080	0.0538	0
	<i>Li</i>	0.6320	0.1227	0.1171	0.0316	0.0967	0
	Improved	0.9991	0.0001	0.0006	0	0.0002	0

theory, our modification shows a better performance in improving the detection accuracy and achieving an accurate CSA of the multi-UAV system.

Nevertheless, the D-S evidence theory still has limitations such as high dependence on original data and lack of solid theoretical foundations. Thus, future work will include heterogeneous multi-sensor fusion, and further improvement of other information fusion methods (e.g. Evidential Reasoning, ER) will also be considered.

Declaration of competing interest

The authors declare that they have no known competing financial interests or personal relationships that could have appeared to influence the work reported in this paper.

Data availability

Data will be made available on request.

Acknowledgements

This work is supported by the China Scholarship Council (Grant No. 202206020114), the Outstanding Research Project of Shen Yuan Honors College (Grant No. 230122204) and the National Natural Science Foundation of China (Grant No. 62303030).

Appendix A. Proof of Lemma 1

Proof. The three properties for $\rho_M(m_i, m_j)$ are proved as follows.

For property 1), we firstly prove the range of ρ_{ij} . According to Cauchy-Schwarz inequality, we have

$$[E(m_i \cdot m_j)]^2 \leq E(m_i^2) E(m_j^2) \quad (\text{A.1})$$

Substituting m_i with $m_i - \mu_{m_i}$, m_j with $m_j - \mu_{m_j}$, we obtain

$$\begin{aligned} & [E((m_i - \mu_{m_i})(m_j - \mu_{m_j}))]^2 \\ & \leq E((m_i - E(m_i))^2) E((m_j - E(m_j))^2) \end{aligned} \quad (\text{A.2})$$

According to (27), we can rewrite (A.2) as

$$\left[\frac{E((m_i - \mu_{m_i})(m_j - \mu_{m_j}))}{\sigma_{m_i} \sigma_{m_j}} \right]^2 = \rho_{ij}^2 \leq 1 \quad (\text{A.3})$$

which is equivalent to

$$-1 \leq \rho_{ij} \leq 1 \quad (\text{A.4})$$

Then, it follows from (29) that

$$\rho_M(m_i, m_j) = \begin{cases} \rho_{ij} \in [0, 1], & \text{if } \rho_{ij} \geq 0, \\ 0, & \text{otherwise.} \end{cases} \quad (\text{A.5})$$

This completes the proof of property 1).

For property 2), we only consider the case of $\rho_{ij} \geq 0$, since $\rho_M(m_i, m_j)$ is zero in the other case. Synthesizing (27) with (28) yields

$$\begin{aligned} \rho_M(m_i, m_j) &= \frac{E((m_i - \mu_{m_i})(m_j - \mu_{m_j}))}{E((m_i - E(m_i))) E((m_j - E(m_j)))} \\ &= \frac{E((m_j - \mu_{m_j})(m_i - \mu_{m_i}))}{E((m_j - E(m_j))) E((m_i - E(m_i)))} \\ &= \rho_M(m_j, m_i) \end{aligned} \quad (\text{A.6})$$

which completes the proof of property 2).

For property 3), we prove its sufficiency (from left to right) firstly, with the consideration of case $\rho_{ij} \geq 0$ ($\rho_M(m_i, m_j)$ is zero if $\rho_{ij} < 0$). Due to $\rho_M(m_i, m_j) = \rho_{ij} = 1$, two standardized versions of m_i and m_j are defined as

$$U = \frac{m_i - E(m_i)}{\sigma_{m_i}}, \quad V = \frac{m_j - E(m_j)}{\sigma_{m_j}} \quad (\text{A.7})$$

Then,

$$\begin{aligned} \rho_{ij} &= \text{Cov}(U, V) = \text{Cov}\left(\frac{m_i - E(m_i)}{\sigma_{m_i}}, \frac{m_j - E(m_j)}{\sigma_{m_j}}\right) \\ &= \text{Cov}\left(\frac{m_i}{\sigma_{m_i}}, \frac{m_j}{\sigma_{m_j}}\right) \\ &= \frac{\text{Cov}(m_i, m_j)}{\sigma_{m_i} \sigma_{m_j}} \end{aligned} \quad (\text{A.8})$$

Using the following inequality

$$\alpha\beta \leq \frac{\alpha^2 + \beta^2}{2}, \quad \forall \alpha, \beta \in \mathbb{R} \quad (\text{A.9})$$

This is because $(\alpha - \beta)^2 \geq 0$. The equality holds only if $\alpha = \beta$. From this, we can obtain that for any two random variables U and V ,

$$E[UV] \leq \frac{EU^2 + EV^2}{2}, \quad (\text{A.10})$$

where the equality holds only if $U = V$ with probability one. Now, let U and V be the standardized versions of m_i and m_j as defined in (A.7). Then, we have $\rho_{ij} = \text{Cov}(U, V) = E[UV]$. Since $EU^2 = EV^2 = 1$, we can derive

$$\rho_{ij} = E[UV] \leq \frac{EU^2 + EV^2}{2} = 1 \quad (\text{A.11})$$

where the equality holds only if $U = V$, i.e.,

$$\frac{m_i - E(m_i)}{\sigma_{m_i}} = \frac{m_j - E(m_j)}{\sigma_{m_j}} \quad (\text{A.12})$$

which implies

$$\begin{aligned} m_j &= \frac{\sigma_{m_j}}{\sigma_{m_i}} m_i + \left(E(m_j) - \frac{\sigma_{m_j}}{\sigma_{m_i}} E(m_i) \right) \\ &= am_i + b, \end{aligned} \quad (\text{A.13})$$

where $a = \sigma_{m_j}/\sigma_{m_i}$ and $b = (E(m_j) - \sigma_{m_j}/\sigma_{m_i} E(m_i))$ are constants. This completes the proof of sufficiency of property 3). The proof of necessity is the reverse process of the above. Note that $\rho_M(m_i, m_j) = 1$ implies that m_j is highly linear with m_i , i.e., evidences m_i and m_j are mutually supportive. So far, we have completed the proof of three properties. ■

References

- [1] Y. He, Mission-driven autonomous perception and fusion based on UAV swarm, *Chin. J. Aeronaut.* 33 (11) (2020) 2831–2834.
- [2] G. Fasano, D. Accardo, A.E. Tirri, A. Moccia, E. De Lellis, Radar/electro-optical data fusion for non-cooperative UAS sense and avoid, *Aerosp. Sci. Technol.* 46 (2015) 436–450.
- [3] C. Han, Y. Gu, X. Sun, S. Liu, Rapid algorithm for covariance ellipsoid model based collision warning of space objects, *Aerosp. Sci. Technol.* 117 (2021) 106960.
- [4] E. Moradi-Pari, A. Tahmasbi-Sarvestani, Y.P. Fallah, A hybrid systems approach to modeling real-time situation-awareness component of networked crash avoidance systems, *IEEE Syst. J.* 10 (1) (2014) 169–178.
- [5] C. Marcus, Aspects of the design, evaluation and accuracy of airborne sensor clusters using time-difference of arrival, *Aerosp. Sci. Technol.* 92 (2019) 892–900.
- [6] T. Nguyen, C.P. Lim, N.D. Nguyen, L. Gordon-Brown, S. Nahavandi, A review of situation awareness assessment approaches in aviation environments, *IEEE Syst. J.* 13 (3) (2019) 3590–3603.
- [7] H. Baek, J. Lim, Design of future UAV-relay tactical data link for reliable UAV control and situational awareness, *IEEE Commun. Mag.* 56 (10) (2018) 144–150.
- [8] Z. Zhen, P. Zhu, X. Yixuan, Y. Ji, Distributed intelligent self-organized mission planning of multi-UAV for dynamic targets cooperative search-attack, *Chin. J. Aeronaut.* 32 (12) (2019) 2706–2716.
- [9] A. Islam, S.Y. Shin Bus, A blockchain-enabled data acquisition scheme with the assistance of UAV swarm in internet of things, *IEEE Access* 7 (2019) 103231–103249.
- [10] J.N. Ho, S.J. Yoo, PSO-based dynamic UAV positioning algorithm for sensing information acquisition in wireless sensor networks, *IEEE Access* 7 (2019) 77499–77513.
- [11] R. Geraldes, A. Goncalves, T. Lai, M. Villerabel, W. Deng, A. Salta, K. Nakayama, Y. Matsuo, H. Prendinger, UAV-based situational awareness system using deep learning, *IEEE Access* 7 (2019) 122583–122594.
- [12] D. Liu, W. Bao, X. Zhu, B. Fei, Z. Xiao, T. Men, Vision-aware air-ground cooperative target localization for UAV and UGV, *Aerosp. Sci. Technol.* 124 (2022) 107525.
- [13] F. Causa, R. Opronolla, G. Fasano, Closed loop integration of air-to-air visual measurements for cooperative UAV navigation in GNSS challenging environments, *Aerosp. Sci. Technol.* (2022) 107947.
- [14] Y. Zhang, X. Wang, S. Wang, X. Tian, Distributed bearing-based formation control of unmanned aerial vehicle swarm via global orientation estimation, *Chin. J. Aeronaut.* 35 (1) (2022) 44–58.
- [15] H. Zhu, J. Li, Y. Gao, G. Cheng, Consensus analysis of UAV swarm cooperative situation awareness, in: Proc. of the 2020 International Conference on Virtual Reality and Intelligent Systems, ICVRIS, IEEE, 2020, pp. 415–418.
- [16] Y. Yu, J. Yu, Y. Liu, Z. Ren, Distributed state estimation for heterogeneous mobile sensor networks with stochastic observation loss, *Chin. J. Aeronaut.* 35 (2) (2022) 265–275.
- [17] J. Wu, K. Ota, M. Dong, J. Li, H. Wang, Big data analysis-based security situational awareness for smart grid, *IEEE Trans. Big Data* 4 (3) (2016) 408–417.
- [18] C. Yang, D. Wang, Y. Zeng, Y. Yue, P. Siritanawan, Knowledge-based multimodal information fusion for role recognition and situation assessment by using mobile robot, *Inf. Fusion* 50 (2019) 126–138.
- [19] C. Kwon, I. Hwang, Sensing-based distributed state estimation for cooperative multiantenna systems, *IEEE Trans. Autom. Control* 64 (6) (2018) 2368–2382.
- [20] A.T. Kamal, J.A. Farrell, A.K. Roy-Chowdhury, Information weighted consensus filters and their application in distributed camera networks, *IEEE Trans. Autom. Control* 58 (12) (2013) 3112–3125.
- [21] H. Ji, F.L. Lewis, Z. Hou, D. Mikulski, Distributed information-weighted Kalman consensus filter for sensor networks, *Automatica* 77 (2017) 18–30.
- [22] J.A. Massignan, J.B. London, M. Bessani, C.D. Maciel, R.Z. Fanucchi, V. Miranda, Bayesian inference approach for information fusion in distribution system state estimation, *IEEE Trans. Smart Grid* 13 (1) (2021) 526–540.
- [23] D. Gaglione, G. Soldi, F. Meyer, F. Hlawatsch, P. Braca, A. Farina, M.Z. Win, Bayesian information fusion and multitarget tracking for maritime situational awareness, *IET Radar Sonar Navig.* 14 (12) (2020) 1845–1857.
- [24] Y. Li, S. Yao, R. Zhang, C. Yang, Analyzing host security using D-S evidence theory and multisource information fusion, *Int. J. Intell. Syst.* 36 (2) (2021) 1053–1068.
- [25] Y. Pan, L. Zhang, X. Wu, M.J. Skibniewski, Multi-classifier information fusion in risk analysis, *Inf. Fusion* 60 (2020) 121–136.
- [26] C. Lu, S. Wang, X. Wang, A multi-source information fusion fault diagnosis for aviation hydraulic pump based on the new evidence similarity distance, *Aerosp. Sci. Technol.* 71 (2017) 392–401.
- [27] W. Cao, S. Xu, A workflow based multi-UAV cooperation architecture, in: Proc. of the 2017 3rd International Conference on Information Management, ICIM, IEEE, 2017, pp. 496–499.
- [28] M. Julio, M.C. Guillermo, B.G. Edgard, B. Everardo, Data fusion as source for the generation of useful knowledge in context-aware systems, *J. Intell. Fuzzy Syst.* 34 (5) (2018) 3165–3176.
- [29] Z. Yao, M. Li, Z. Chen, R. Zhou, Mission decision-making method of multi-aircraft cooperatively attacking multi-target based on game theoretic framework, *Chin. J. Aeronaut.* 29 (6) (2016) 1685–1694.
- [30] Y. Zhang, Q. Xiao, X. Deng, W. Jiang, A multi-source information fusion method for ship target recognition based on Bayesian inference and evidence theory, *J. Intell. Fuzzy Syst.* 42 (Preprint) (2022) 1–16.
- [31] Z. Lin, J. Xie, Research on improved evidence theory based on multi-sensor information fusion, *Sci. Rep.* 11 (1) (2021) 1–6.
- [32] P. Smets, The combination of evidence in the transferable belief model, *IEEE Trans. Pattern Anal. Mach. Intell.* 12 (5) (1990) 447–458.
- [33] R.R. Yager, On the Dempster-Shafer framework and new combination rules, *Inf. Sci.* 41 (2) (1987) 93–137.
- [34] Q. Sun, X. Ye, W. Gu, A new combination rules of evidence theory, *Acta Electron. Sin.* 28 (8) (2000) 117.
- [35] C.K. Murphy, Combining belief functions when evidence conflicts, *Decis. Support Syst.* 29 (1) (2000) 1–9.
- [36] T. Horiuchi, Decision rule for pattern classification by integrating interval feature values, *IEEE Trans. Pattern Anal. Mach. Intell.* 20 (4) (1998) 440–448.
- [37] Y. Li, J. Chen, F. Ye, D. Liu, The improvement of DS evidence theory and its application in IR/MMW target recognition, *J. Sens.* (2016) 1–15.
- [38] J. Du, X. Hu, M. Krstic, Y. Sun, Robust dynamic positioning of ships with disturbances under input saturation, *Automatica* 73 (2016) 207–214.
- [39] A.P. Dempster, Upper and lower probabilities induced by a multivalued mapping, in: *Classic Works of the Dempster-Shafer Theory of Belief Functions*, Springer, 2008, pp. 57–72.
- [40] A.M. Pinto, P. Costa, A.P. Moreira, L.F. Rocha, G. Veiga, E. Moreira, Evaluation of depth sensors for robotic applications, in: Proc. of the 2015 IEEE International Conference on Autonomous Robot Systems and Competitions, IEEE, 2015, pp. 139–143.
- [41] E.H. Matsushima, A.P. de Oliveira, N.P. Ribeiro-Filho, J.A. Da Silva, Visual angle as determinant factor for relative distance perception, *Psicológica* 26 (1) (2005) 97–104.